Lumped Elements Loaded Miniaturized Antenna for Bluetooth Enabled Hearing Aid Devices

by

Zhichao Li

A thesis

presented to the University of Waterloo

in fulfillment of the

thesis requirement for the degree of

Master of Applied Science

in

Electrical and Computer Engineering

Waterloo, Ontario, Canada, 2016

AUTHOR'S DECLARATION

I hereby declare that I am the sole author of this thesis. This is a true copy of the thesis, including any required final revisions, as accepted by my examiners.

I understand that my thesis may be made electronically available to the public.

Abstract

Hearing loss is one of the most common physical and sensory impairments among all ages, especially elders. Hearing loss may affect only one ear or both ears of a patient at a different degree of impairment. This asymmetrical nature of hearing loss makes it more difficult for the patient to localize the source of the sound properly. One possible solution for this asymmetry of hearing problem is to use a pair of hearing aid devices. Each hearing aid device should be able to deal with such asymmetry of the ears, as well as the natural asymmetry induced by spectral sound differences. By using a pair of hearing aid devices operating at 2.4GHz- 2.5GHz Bluetooth band, wirelessly communicating with each other, the binaural processing will be improved for the person who suffers from unbalanced hearing loss between the two ears and one can properly localize the source of the sound.

A novel lumped elements loaded miniaturized differential dipole antenna for Bluetooth enabled hearing aid devices is proposed. Miniaturization of the proposed antenna is achieved by planting lumped components directly on the optimized locations of the antenna traces. The lumped elements also serve as a matching circuit which matches the antenna's input impedance directly to the radio, without need for an additional dedicated matching circuit. The effect of the human body is taken into consideration during the antenna design stages. The proposed antenna was simulated, fabricated and measured. There are some good agreements between simulated and measured results. Radio link tests were done after integrating the proposed antenna with a hearing aid package, and good link ranges were observed. Integrating tunable elements, for example voltage controlled capacitors; directly on the antenna structure to achieve adaptive matching according to different human bodies will be a valuable future work for this research.

Acknowledgements

I would like to give my sincere appreciation to my supervisor, Prof. Safieddin Safavi-Naeini, for his guidance and support throughout my entire master's program. I am really thankful for having such a great opportunity to learn from such a talented and knowledgeable professor. It's amazing that he has been so patient and given me the full trust for these two years in his research group. I learned a lot from the research project meetings we had and the three graduate courses that he taught. And I'd also like to give my thanks to Prof. Safavi-Naeini for giving me the opportunity to be his TA when he taught the undergraduate course ECE-474. I had such a great time working with and learning from him.

Special thanks go to Dr. George Shaker who gave me a lot of suggestions on my research project and hands-on help on my measurements. Not only is he a great researcher who has a good knowledge in various areas, but also such a wonderful person who likes to give help to anyone who needs it. His rigorousness in research and humbleness in life will always be respected.

I would also like to give my thanks to Dr. Mohammad-Reza Nazhad-Almadi. He gave me plenty of help on fabricating my antenna samples and testing them. He gave me the full access to the lab at On Semiconductor and taught me how to use the software for measuring antenna radiation pattern. He also helped me when I was doing the radio link tests.

It's a great honor to learn the course ECE-738 from Prof. Bosco Leung. It was the first graduate course I took at University of Waterloo and Prof. Leung helped me get through the transformation time. And I want to give my sincere thanks to Prof. Andrei Sazonov who taught me the course ECE-632. It was fun to explore a brand new area with his help.

And I really appreciate that Prof. Omar Ramahi and Prof. Dayan Ban who gave me the opportunity to serve as TA for their undergraduate courses ECE-475 and NE-241, respectively. I have learned a lot from them and I had a great time with their undergraduate students. It's always fun to see how other students solve problems and many of those students became my friends.

I had a wonderful time with my fellow researchers in CIARS group. Many thanks to my good friends Ray Chen and Luxsumi Jeevananthan, they helped me a lot on my study and daily life ever since I knew them. I had a cheerful time with them and hopefully our friendship will last a life time. I am grateful to Dr. Gholamreza Zeinolabedin Rafi who gave me lots of help in the measurements of my antennas. And I want to give thanks to Dr. Aidin Taeb for teaching me how to use the equipment in the labs. I would also like to thank Mr. Behrooz Semnani for being such a patient TA when I took the courses ECE-675 and ECE-770. I cannot forget the contribution by Mr. Mohammadsadegh Faraji-Dana on simplifying the complex human body model. And it's great to have the chance working on the same project with Miss. Sung Eun Kim and Ms. Shadi Dashmiz. I must give my appreciation to the others in CIARS group, Dr. Shahed Shahir, Dr. Ahmed Ibrahim Nashed, Mr. Hamed Holisaz, Mr. Mohammad Haghtalab, Dr. Mehdi Salehi, Mr. Hussam Al-Saedi, Miss. Naimeh Ghafarian, Dr. Mahmoud Niroojazi, Mr. Danish Khan, Dr. Suren Gigoyan, Mr. Mohammadbagher Fereidani Samani, Mr. Stanley Omokhudu Ituah, Dr. Wael Abdelwahab, Dr. Nazy Ranjkesh, Mr. Hadi Amarloo, Mr. Seyyed Mohsen Raeis Zadeh Bajestani, and Mr. Yilong Zhang. I learned a lot from all of you during our weekly group meeting.

This research was supported by National Science and Engineering Research Council (NSERC) of Canada, International Science and Technology Partnership (ISTP) Canada and On Semiconductor. Special thanks to these organizations for their support on our research work.

Although these chats were irrelevant to this thesis work, I have to give my special appreciation to my following friends I had a pleasant time with Ms. Haining Cao, Tony Li, Hao Zhang, Mingjun Gao, Liang Dong, Yiling Xu, Randy Xing, Zhuoran Yin, Yunling Cui, Ruixue Zhang, Nansen Lin, Yi San, Xulai Cao and so on. It's because of their companion and encouragement among these two years that I enjoyed my life here so much.

Many thanks go to my uncle Dr. Zhongshun Yuan. It was because of him that I applied the master program at University of Waterloo. He gave me lots of suggestions and helped on my application. If it wasn't for him, I would not have this opportunity of studying at University of Waterloo. And I really appreciate his whole family who treated me as one of their own family members ever since I came to Canada. I would like to give thanks to my cousin Michael Yuan for being such a good relative and friend to me.

Lastly and mostly, I would like to give my sincere thanks to my whole family, my grandfather, my father, my brother and sister-in-law, my uncles and aunts, back in China who are always there for me. Their love, faith and support keep me going and remind me to be a better person all the time. I cannot tell how much I love my mother in heaven and it was her who made me the person I am today. Her love, faith, and optimism in life and her family even when she was really ill had a major influence on me. I am trying my best to make her proud of me.

Table of Contents

List of Figures

List of Tables

Chapter 1. Introduction

1.1 Introduction to Body Area Network

A body area network (BAN), also referred to as a wireless body area network (WBAN) or a body sensor network, is a wireless network of wearable computing devices. BAN devices are devices embedded inside the body, surface-mounted on the body in a fixed position or they can be accompanied devices which human can carry in different positions, in cloth pockets, by hand or in various bags [1].

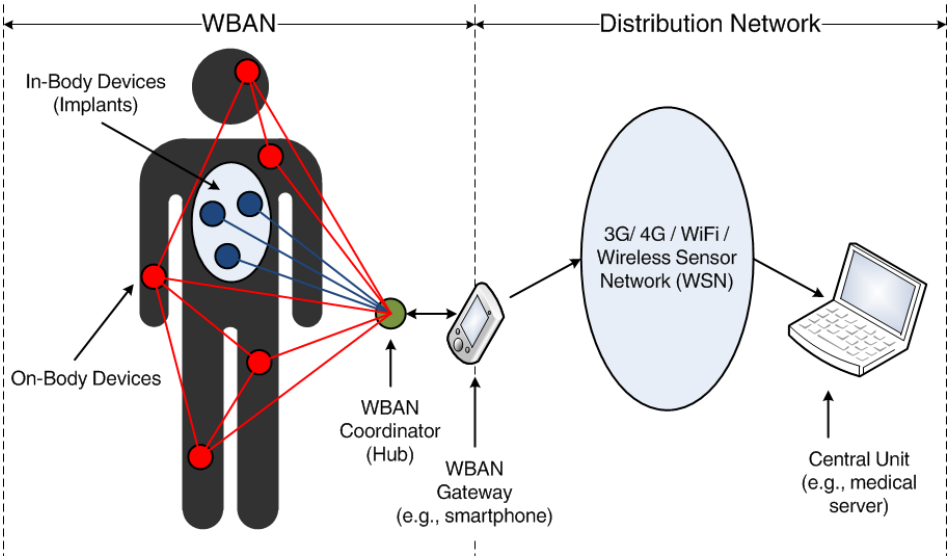

Fig. 1.1. Body Area Network (BAN)

There is a trend towards the miniaturization of such devices, in particular, networks consisting of several miniaturized body sensor units together with a single body central unit [2-3]. However, larger decimeter sized smart devices, accompanied devices, still play an important role by acting as a data hub, data gateway and providing a user interface to view and manage BAN applications. The development of WBAN technology started around 1995 where the idea of using wireless personal area network technologies to implement communications on, near, and around the human body occurred. Few years later, the term “BAN” came to refer systems where communication is entirely within, on, and in the immediate proximity of a human body [4-5]. A BAN system can use wireless personal area network technologies as gateways to reach longer ranges. Through these gateway

devices, it is possible to connect the wearable devices on the human body to the internet. This way, medical professionals can access patient data online using the internet independent of the patient location as shown in Fig. 1.1[6].

This research focuses on the development of intelligent wireless sensors that can adapt and optimize their performance while operating in, on or around the human body. One application of this research project is wireless hearing aids.

1.2 Introduction to Some Hearing Problems and Proposed Solution

Hearing lost is one of the most common physical and sensory impairments among all ages, especially elders as shown in Fig. 1.2 [7]. Not being able to see a hearing loss directly makes this disease an "invisible" condition, whose side effects can only be observed upon behavior and communication [8-9]. Those side effects which vary from one person to another, makes hearing loss such a complicated disease which is responsible for the pressure, anxieties and conflicts happened in one's life.

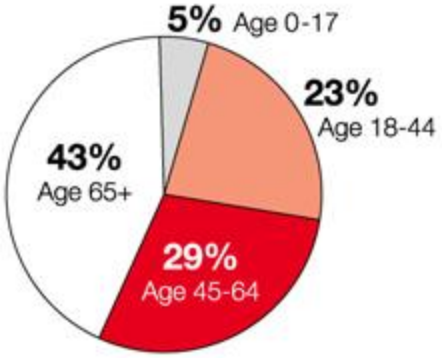

Fig. 1.2. Who has hearing loss?

Binaural processing, in audiology, is the capability of the brain to process sound coming from both the left and the right ears which helps in localizing the source of the sound [10]. Hearing loss has an asymmetrical nature and it may affect only one ear or both ears of a patient at a different degree of impairment as demonstrated in Fig. 1.3[6]. The asymmetrical nature of hearing loss makes it more difficult for a patient to localize the source of the sound properly.

(a) (b)

Fig. 1.3. Asymmetrical nature of hearing loss: (a) Single ear; (b) Both ears

One possible solution for this asymmetry is to use a pair of hearing aid devices. Each hearing aid device should be able to deal with such asymmetry of the ears, as well as the natural asymmetry induced by spectral sound devices. By using a pair of hearing aid devices operating at 2.4 GHz-2.5GHz Bluetooth frequency band, wirelessly communicating with each other, the binaural processing will be improved for a person who suffers from unbalanced hearing loss and he or she can properly localize the source of the sound [11].

Generally speaking, there are two different types of hearing aid devices with respect to the location where people put them on as shown in Fig. 1.4[6]. The first type goes inside one's ears, and the second type goes behind one's ears. And we choose the behind ear configuration for our application.

(a) (b)

Fig. 1.4. Two types of hearing aids: (a) Inside ear configuration; (b) Behind ear configuration

1.3 Organization of the Dissertation

The objective of this dissertation is to design a miniaturized antenna operating at ISM band to meet the needs of individuals suffering from unbalanced hearing. One essential part of wireless hearing aid application is to design miniaturized antenna which can operate in the proximity of a human body with omnidirectional radiation pattern and acceptable antenna efficiency. Works have been done in designing antenna for near head applications [12-20] and modelling propagation channel in or around the human head [21-25]. Here, we proposed a lumped elements loaded miniaturized antenna for Bluetooth enabled hearing aid devices.

Theory of mixed-mode scattering parameters is reviewed in chapter two. The transformation between the standard scattering parameters and the mixed-mode scattering parameters is required because we choose the differential signal for our application to achieve better noise performance. There is no direct way to measure a differential signal by a normal vector network analyzer, so the transformation is utilized.

Designs, simulations and measurements of a lumped inductors loaded miniaturized differential dipole antenna are illustrated in chapter three. Challenges in the design of an antenna for hearing aid devices are introduced in section 3.1. Dipole antenna was chosen for this application to achieve omnidirectional radiation requirement. Simulation results of the designed antenna in free space (section 3.2) and with the presence of human head (section 3.3) show that designed antenna meets the other requirements as well. Designed antenna was fabricated and measured. Measurement results (section 3.4) have good agreements with the simulation results, which means the idea of loading inductors directly on the antenna structure is applicable.

Then, integration of a lumped capacitors loaded symmetrical dipole antenna with radio board package for a finalized hearing aid case focusing on ear-to-remote communication application is demonstrated in chapter four. Section 4.1 introduces a lumped capacitors loaded symmetrical differential dipole antenna which can satisfy the limited allocated PCB space for the antenna. Then, a brief introduction of integrating the designed antenna with a radio board designed by On Semiconductor into a finalized hearing aid case is demonstrated in section 4.2. Radio link tests between this hearing aid device and a cellphone were conducted and good link ranges were observed.

Chapter five concludes this research study addressing future. A brief note is given on possible realization in integrating tunable elements, for example voltage controlled capacitors, directly on the antenna structure to achieve adaptive matching for BAN applications.

Chapter 2. Theory of Mixed-mode Scattering Parameters

Differential signaling is the primary choice for a low power RF circuit, since it provides superior immunity to noise by offering twice the signal swing for a given supply voltage. Moreover, the out of phase property of a balanced pair has several other benefits: "it rejects any common mode interference signal, cancels the even order distortions, and reduces Electromagnetic Interference (EMI), EMI emission, and susceptibility" [26]. Considering these advantages, the RF and antenna part of our hearing aid device are designed to be in a differential configuration. To do so, the transformation between the standard scattering parameters and the mixed-mode scattering parameters is required.

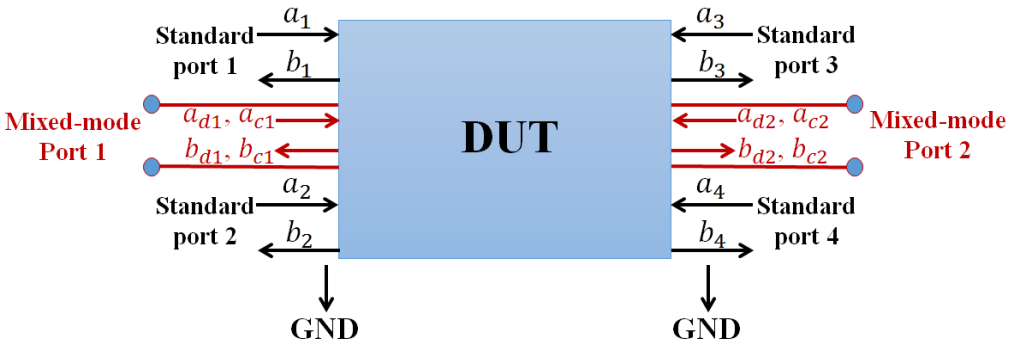

Fig. 2.1. Diagram of a general two-port differential circuit

D. E. Bockelman, et. al. developed the method to convert the standard scattering parameters into mixed-mode scattering parameters [27]-[28]. Consider the differential circuit composed by two differential ports as shown in Fig. 2.1. The incident waves and reflected waves of a standard four ports network are represented by a_1, a_2, a_3, a_4 and b_1, b_2, b_3, b_4 respectively. Standard port 1 and port 2 construct mixed-mode port 1, and standard port 3 and port 4 construct mixed-mode port 2. According to [28], the normalized differential-mode incident and reflected waves are represented by a_{d1}, a_{d2} and b_{d1}, b_{d2} respectively. Similarly, the normalized common-mode incident and reflected waves are represented by a_{c1}, a_{c2} and b_{c1}, b_{c2}.

The mixed-mode normalized waves can be written in terms of standard normalized waves as [28]:

$$
\begin{aligned}
a_{d1} &= \frac{1}{\sqrt{2}}(a_1 - a_2), \quad a_{d2} = \frac{1}{\sqrt{2}}(a_3 - a_4) \\
a_{c1} &= \frac{1}{\sqrt{2}}(a_1 + a_2), \quad a_{c2} = \frac{1}{\sqrt{2}}(a_3 + a_4) \\
b_{d1} &= \frac{1}{\sqrt{2}}(b_1 - b_2), \quad b_{d2} = \frac{1}{\sqrt{2}}(b_3 - b_4) \\
b_{c1} &= \frac{1}{\sqrt{2}}(b_1 + b_2), \quad b_{c2} = \frac{1}{\sqrt{2}}(b_3 + b_4)
\end{aligned}
\tag{1}
$$

Rewrite (1) in the matrix form, we get (2)-(3).

$$
\begin{bmatrix} a_{d1} \\ a_{d2} \\ a_{c1} \\ a_{c2} \end{bmatrix} = \frac{1}{\sqrt{2}} \begin{bmatrix} 1 & -1 & 0 & 0 \\ 0 & 0 & 1 & -1 \\ 1 & 1 & 0 & 0 \\ 0 & 0 & 1 & 1 \end{bmatrix} \begin{bmatrix} a_1 \\ a_2 \\ a_3 \\ a_4 \end{bmatrix} = M \begin{bmatrix} a_1 \\ a_2 \\ a_3 \\ a_4 \end{bmatrix} \tag{2}
$$

$$
\begin{bmatrix} b_{d1} \\ b_{d2} \\ b_{c1} \\ b_{c2} \end{bmatrix} = \frac{1}{\sqrt{2}} \begin{bmatrix} 1 & -1 & 0 & 0 \\ 0 & 0 & 1 & -1 \\ 1 & 1 & 0 & 0 \\ 0 & 0 & 1 & 1 \end{bmatrix} \begin{bmatrix} b_1 \\ b_2 \\ b_3 \\ b_4 \end{bmatrix} = M \begin{bmatrix} b_1 \\ b_2 \\ b_3 \\ b_4 \end{bmatrix} \tag{3}
$$

Where matrix M in (2)-(3) is defined as:

$$
M = \frac{1}{\sqrt{2}} \begin{bmatrix} 1 & -1 & 0 & 0 \\ 0 & 0 & 1 & -1 \\ 1 & 1 & 0 & 0 \\ 0 & 0 & 1 & 1 \end{bmatrix} \tag{4}
$$

Mixed-mode normalized incident and reflected waves, and standard normalized incident and reflected waves can be related in terms of mixed-mode scattering parameters and standard scattering

parameters, respectively. S_{mm} and S_{std} in (5)-(6) stand for mixed-mode scattering matrix and standard scattering matrix, respectively.

$$\begin{bmatrix} b_{d1} \\ b_{d2} \\ b_{c1} \\ b_{c2} \end{bmatrix} = S_{mm} \begin{bmatrix} a_{d1} \\ a_{d2} \\ a_{c1} \\ a_{c2} \end{bmatrix} = \begin{bmatrix} S_{d1d1} & S_{d1d2} & S_{d1c1} & S_{d1c2} \\ S_{d2d1} & S_{d2d2} & S_{d2c1} & S_{d2c2} \\ S_{c1d1} & S_{c1d2} & S_{c1c1} & S_{c1c2} \\ S_{c2d1} & S_{c2d2} & S_{c2c1} & S_{c2c2} \end{bmatrix} \begin{bmatrix} a_{d1} \\ a_{d2} \\ a_{c1} \\ a_{c2} \end{bmatrix} \tag{5}$$

$$\begin{bmatrix} b_1 \\ b_2 \\ b_3 \\ b_4 \end{bmatrix} = S_{std} \begin{bmatrix} a_1 \\ a_2 \\ a_3 \\ a_4 \end{bmatrix} = \begin{bmatrix} S_{11} & S_{12} & S_{13} & S_{13} \\ S_{21} & S_{22} & S_{23} & S_{24} \\ S_{31} & S_{32} & S_{33} & S_{34} \\ S_{41} & S_{42} & S_{43} & S_{44} \end{bmatrix} \begin{bmatrix} a_1 \\ a_2 \\ a_3 \\ a_4 \end{bmatrix} \tag{6}$$

From (2)-(6), the transformation between standard scattering parameters and mixed-mode scattering parameters is done in (7).

$$S_{mm} = MS_{std}M^{-1} = \begin{bmatrix} S_{d1d1} & S_{d1d2} & S_{d1c1} & S_{d1c2} \\ S_{d2d1} & S_{d2d2} & S_{d2c1} & S_{d2c2} \\ S_{c1d1} & S_{c1d2} & S_{c1c1} & S_{c1c2} \\ S_{c2d1} & S_{c2d2} & S_{c2c1} & S_{c2c2} \end{bmatrix} \tag{7}$$

The differential-mode scattering parameters in (8), obtained from (7), are used in the following chapters.

$$\begin{aligned} S_{d1d1} &= \frac{1}{2}(S_{11} - S_{12} - S_{21} + S_{22}) \\ S_{d1d2} &= \frac{1}{2}(S_{13} - S_{23} - S_{14} + S_{24}) \\ S_{d2d1} &= \frac{1}{2}(S_{31} - S_{32} - S_{41} + S_{42}) \\ S_{d2d2} &= \frac{1}{2}(S_{33} - S_{34} - S_{43} + S_{44}) \end{aligned} \tag{8}$$

As we mentioned before, we need a pair of hearing aids for ear-to-ear communication application, which means that we have two identical antennas in our hearing aid system. And we choose differential dipole antenna for the application because of the advantages of differential signal. As shown in Fig. 2.2, each differential dipole antenna has two standard ports, so that there are four standard ports in total for the hearing aid system. Once we get the standard four-port scattering parameters from simulations or measurements, we can then use formulas illustrated in (8) to calculate the differential return loss of each antenna, and differential insertion loss between two antennas.

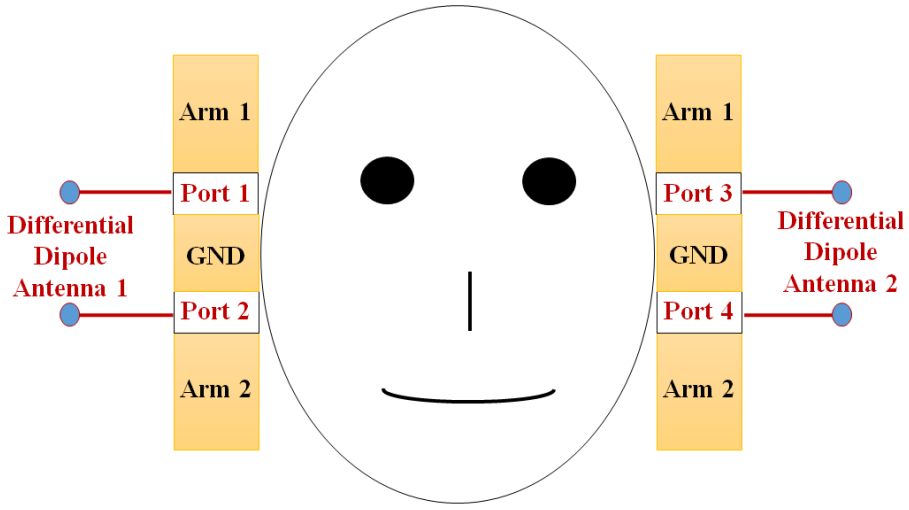

Fig. 2.2. Diagram of a hearing aid system containing two identical differential dipole antennas

Chapter 3. Designs, Simulations and Measurements of a Lumped Inductors Loaded Differential Dipole Antenna for Bluetooth Enabled Hearing Aid Devices

The increasing growth of wireless Bluetooth devices operating at 2.4GHz- 2.5GHz frequency band has attracted industrial companies to incline towards this range of frequency in designing their products. In this chapter, a lumped inductors loaded differential dipole antenna operating at Bluetooth band is proposed to meet the needs of individuals suffering from unbalanced hearing problems.

3.1 Challenges in Antenna Design

The two main challenges in implementing the antenna for a hearing aid device are the limited allocated space for the antenna and the presence of the human head in the proximity of the radiating element. As shown in Fig. 3.1, the available PCB space for the antenna of our first prototype is comparable to a coin. Although the given PCB is a planar structure, it needs to fit into a specific hearing aid case. Thus, flexible substrate which can be bent easily must be chosen in the process of designing the antenna to make sure that it can be integrated with the other parts of a hearing aid device.

Fig. 3.1. Available PCB space for antenna

Considering the fact that the size, shape and even properties of each individual human head are different, optimizing the antenna performance while operating around a human head is the major challenge. So coming up with a novel antenna which can be adjusted for individuals to give customers better user experience would be a valuable work to do. And another thing one must take into consideration is that human body is a highly lossy medium at 2.4GHz- 2.5GHz frequency band, so the designed antenna must have acceptable efficiency at a certain direction to ensure good communication between the left and right ears.

3.2 Designed Antenna and Simulation Results in Free Space

In this section, the major considerations in designing a lumped inductors loaded differential dipole antenna are presented and some simulation results of the designed antenna in free space environment are demonstrated.

3.2.1 Major Considerations in Antenna Design

For a hearing aid antenna, an omnidirectional radiation pattern is needed to support not only ear-to-ear communication application, but also ear-to-remote communication application. Dipole antenna, loop antenna or slot antenna all can be chosen when an omnidirectional radiation pattern is required. But for the given PCB space, the possible loop antenna design for this application will be electrically small loop which is difficult to match. And considering that the available RF ground is small, the slot antenna would not be a good option either. Thus, a dipole antenna is designed to meet this requirement.

Considering all the advantages of differential signals as we mentioned in section 2.1, a dipole antenna with differential feeds is designed. The differences between a differential dipole antenna and a normal dipole antenna are shown in Fig. 3.2. For a normal dipole antenna, there is just one feed port. But for a differential dipole antenna, there are two feed ports which have the same magnitude and are out of phase.

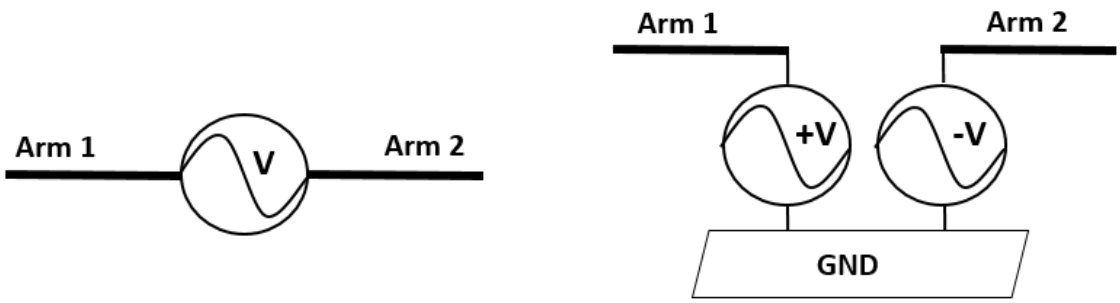

(a) (b)

Fig. 3.2. Dipole antennas: (a) Normal dipole antenna; (b) Differential dipole antenna

3.2.2 Designed Antenna Model

The geometry of proposed inductors loaded differential dipole antenna is shown in Fig. 3.3. From the side view of this antenna model, we can see that the two arms of this dipole antenna are not on the same surface and the two surfaces are separated by a ground with a width of 5mm. There are two feed ports to excite this differential dipole as we mentioned. One feed port was connecting arm 1 with the ground, and another feed port was connecting arm 2 with the ground. These two feed ports had the same magnitude and 180 degrees phase difference of voltages. The battery modeled as a cylinder was connected with ground as it is in reality. The substrate used in this model was flexible material, UL3850 provided by Rogers Corporation. The dielectric constant of this substrate is 2.9 and the thickness of the substrate is 0.1mm. To be assured that the hearing aid device works well when it is inserted on either side of the head (left/right ear), the proposed antenna was designed in such a way to conform to the natural symmetries, in term of line width and the total length.

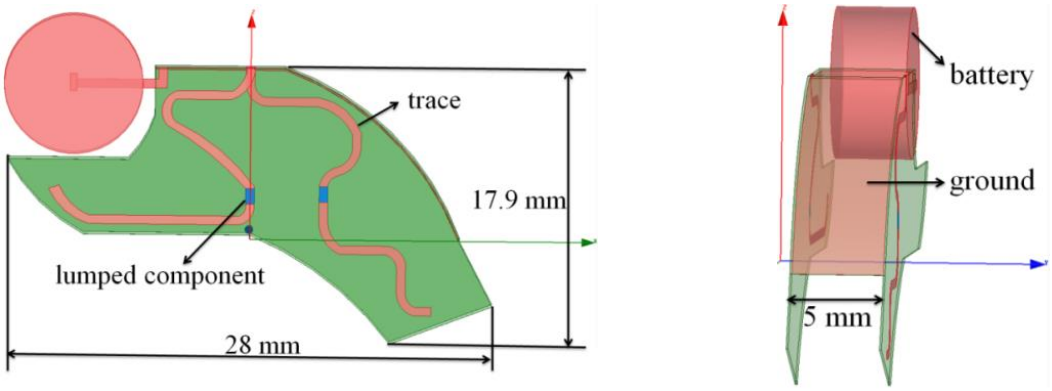

(a) (b)

Fig. 3.3. Geometry of proposed antenna: (a) Front view; (b) Side view

3.2.3 Resonant Frequency VS Inductances

The inductive lumped components are planted at the center of the two antenna traces, as shown in Fig. 3.4. Not only do they reduce the necessary length of the trace at certain bands, but they also serve as matching circuits to match the input impedance of antennas to the input/output radio. Using this strategy would also save the space for any additional matching circuit which was going to be employed between the radio and the antenna.

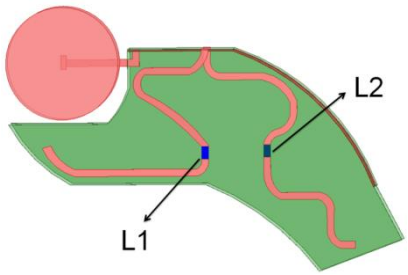

Fig. 3.4. Locations of implanted inductors on the antenna arms

Choosing locations for implanting the lumped inductors was a process of trade-off between the total length and the radiation efficiency of the antenna. A model of a simple printed dipole antenna with loaded inductors in HFSS is shown in Fig. 3.5. Two 3nH lumped inductors were implanted on the two

arms of the dipole antenna, symmetrically about the excitation port. The distance between the locations of the excitation port and one lumped inductor was a variable d (if d=0, that means there were no lumped components loaded on the antenna structure). As we can see from Fig. 3.6, as the distance between the locations of the excitation port and the lumped inductor decreases, the resonant frequency of the antenna shifts to the lower band and the radiation efficiency of the antenna decreases in the meantime. Implanting lumped inductors on the antenna structure surely can reduce the total length of the antenna at a desired band, but it also sacrifices a certain amount of radiation efficiency of the antenna. Considering that the available PCB size for the antenna is limited in this design and one does not want to sacrifice too much efficiency, the optimal locations for implanting the lumped components would be at the centers of the two antenna arms.

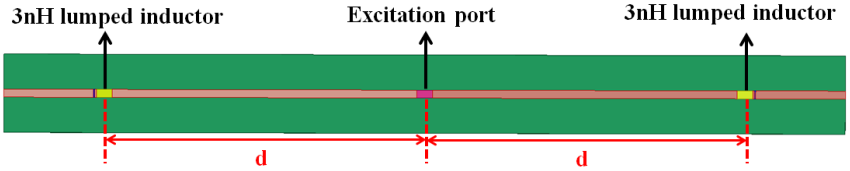

Fig. 3.5. Model of a simple printed dipole antenna with loaded lumped inductors

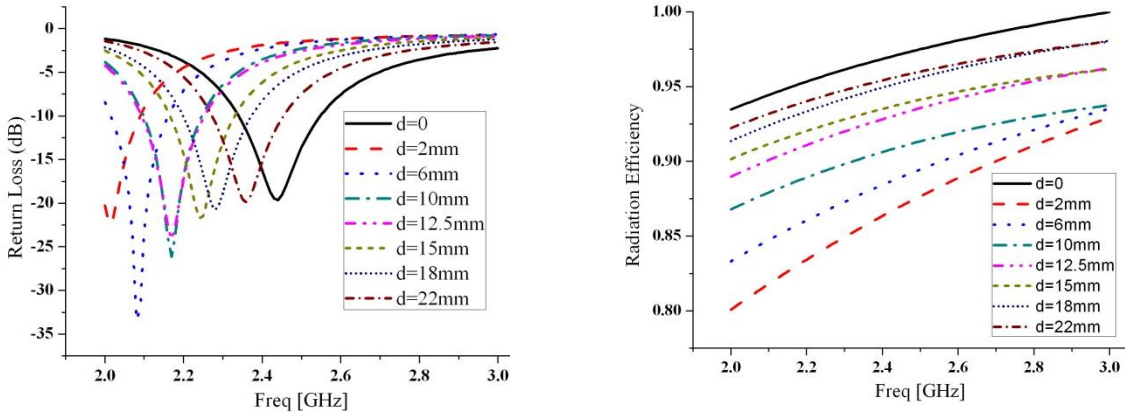

(a) (b)

Fig. 3.6. Effects of the locations of the lumped inductors on: (a) Return loss; (b) Radiation efficiency

Furthermore, we chose three different locations to implant lumped inductor L1 to verify whether the optimal location for the designed hearing aid antenna was at the center of the trace or not. As shown

in Fig. 3.7, the three chosen locations were close to the excitation port, at the center of the trace, or close to the end of the trace, respectively. And the capacitance of L1 keeps unchanged. As we can see from Fig. 3.8, as the location to implant L1 moves further to the excitation port, the resonant frequency shifts to higher band and the radiation efficiency increases. So taking resonant frequency and radiation efficiency into consideration at the same time, the optimal location was at the center of the trace.

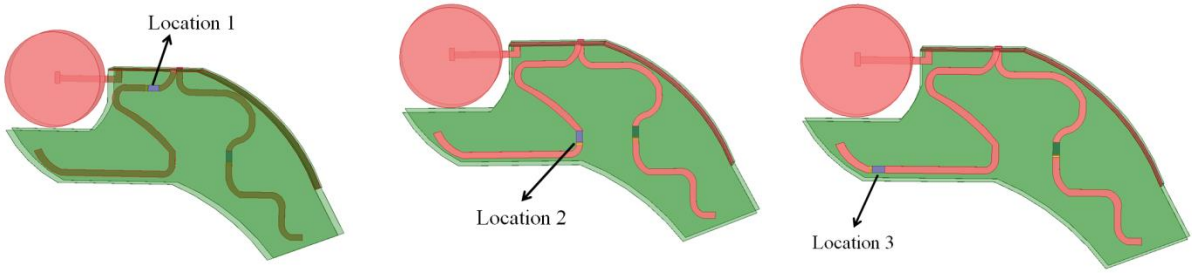

(a) (b) (c)

Fig. 3.7. Three different locations to implant L1: (a) Close to the excitation port; (b) At the center of the trace; (c) Close to the end of the trace

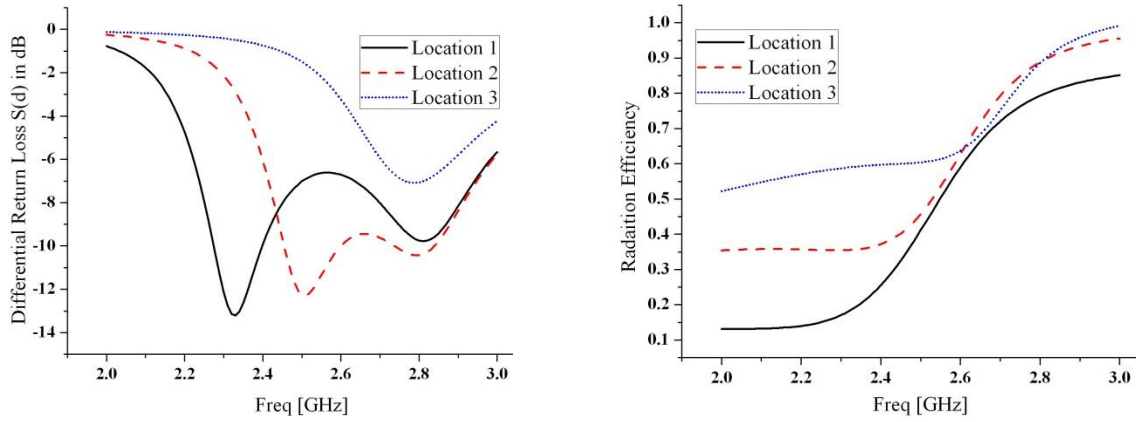

(a) (b)

Fig. 3.8. Three different locations to implant L1: (a) Differential return loss S(d); (b) Radiation efficiency

For a differential feed dipole antenna, the differential return loss S(d) can be obtained from a general two port scattering matrix as mentioned in section 2.1. As shown in Fig. 3.9, the resonant frequency

of this differential dipole antenna can be easily adjusted by changing the inductance values of these two lumped inductors, L1 and L2. As we expected, the resonant frequency would shift down as the inductance of either L1 or L2 increases. The beauty of having two inductors is that we have two degrees of freedom to change the antenna impedance, which are very beneficial considering the fact that we need to match the antenna impedance to the radio with the presence of human head. Matching the antenna impedance to the radio in free space environment is not necessary since we know that the presence of human head while the hearing aid device is operating would cause changes on the antenna impedance. As we will discuss the effects of battery in antenna model, antenna radiation pattern and radiation efficiency in the following parts, a set of fixed values of lumped inductors L1 and L2, which are 3.6nH and 0.1nH respectively, have been chosen. The reason of choosing this set of values is that the antenna impedance is matched to the radio with the presence of the human head with the chosen values of L1 and L2.

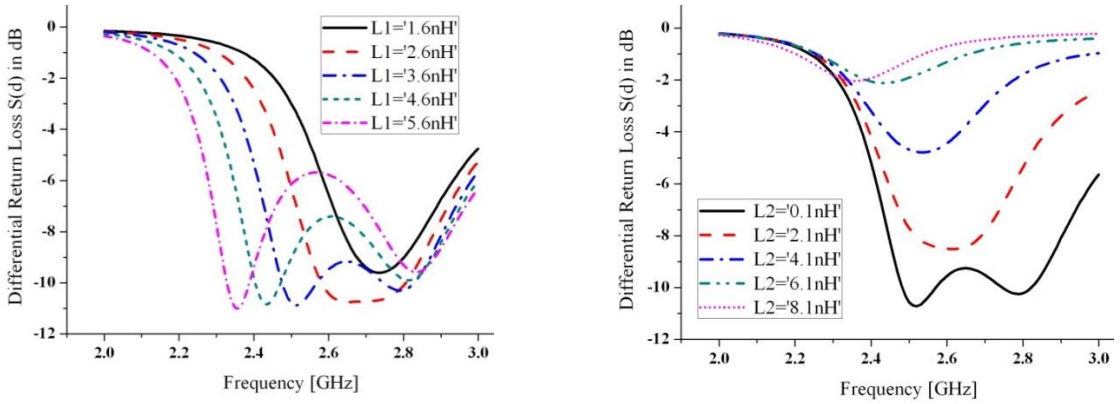

(a) (b)

Fig. 3.9. Resonant frequency VS inductances: (a) Varying L1; (b) Varying L2

3.2.4 Effects of Battery in the Antenna Model

In order to study the effects of battery in the antenna model, we made comparisons on the differential return loss, S(d), and differential impedance, Z(d), of complete antenna model (finalized model including the battery) and incomplete model (without battery). Including the battery, which was connected to the ground, caused a shift in the resonant frequency of the dipole to the lower frequency band as shown in Fig. 3.10. This effect has been carefully taken into the consideration in the design of

the final prototype of the antenna. To minimize the coupling from the battery and the ground, the traces of the two arms of the antenna should be kept as far as possible away from them.

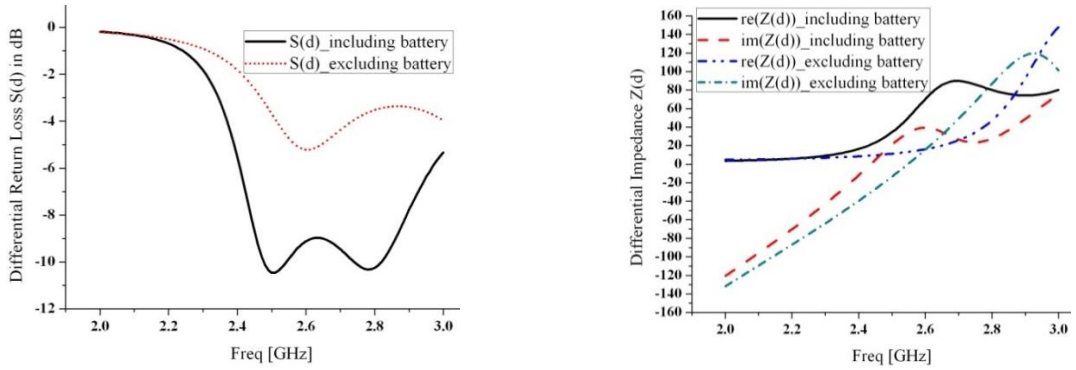

(a) (b)

Fig. 3.10. Effects of battery on: (a) Differential return loss S(d); (b) Differential impedance Z(d)

3.2.5 Radiation Pattern and Radiation Efficiency

Fig. 3.11 shows the current distribution on antenna arms, ground and battery at the resonant frequency which is 2.5GHz. It is obvious that the current on the two antenna arms is much stronger than that on the ground or battery, and major radiation will be caused by these two arms of the antenna. The radiation pattern of this current distribution will be similar to a dipole lying on the xoz plane. As shown in Fig. 3.12, an omnidirectional dipole-like radiation pattern is observed at not only resonant frequency 2.5GHz, but also at its two sidebands, 2.45GHz and 2.55GHz.

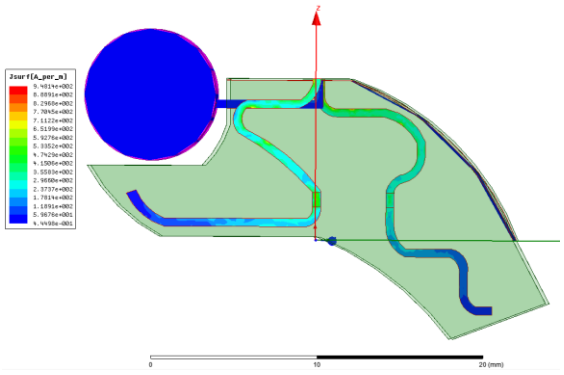

Fig. 3.11. Current distribution at resonant frequency

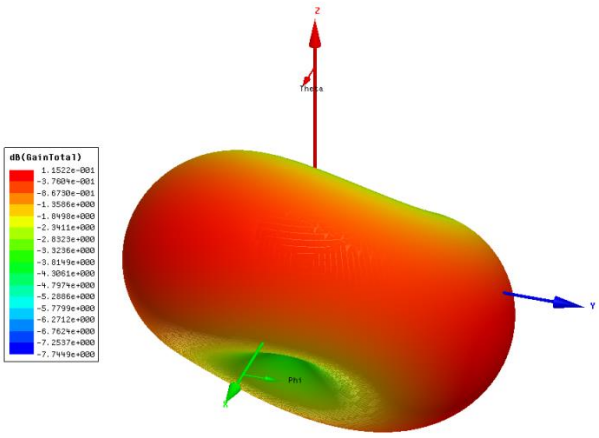

(a)

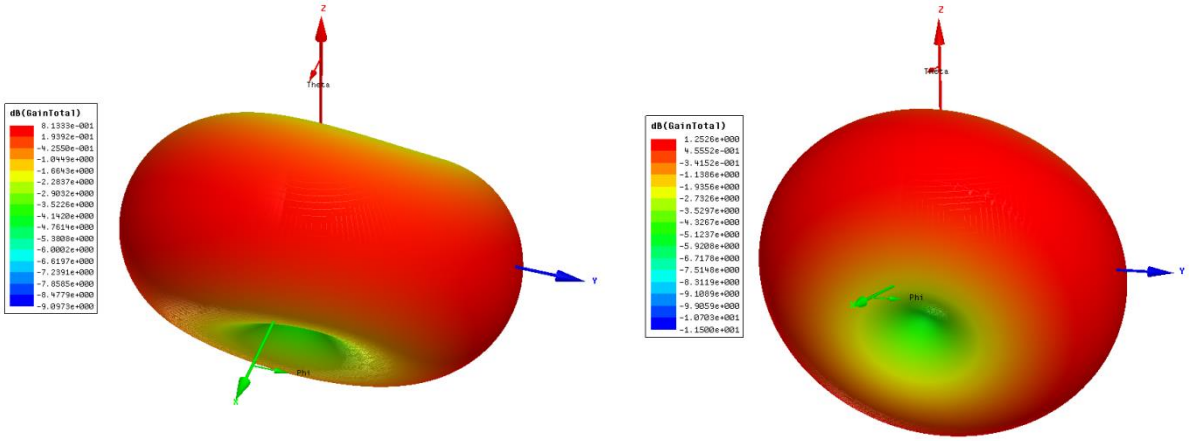

(b) (c)

Fig. 3.12. Radiation pattern at different frequencies: (a) 2.5GHz; (b) 2.45GHz; (c) 2.55GHz

The two lumped inductors loaded directly on the antenna structure would have caused a drop on the antenna radiation efficiency. To study the loss contributed by lumped inductors, quality factors of these inductors must be taken into consideration. Both lumped inductors are 0402 planar inductors with quality factors of 30 which are widely used in the industry. For a lumped inductor:

$$Q = \frac{\omega L}{R} = \frac{2\pi f L}{R} \tag{9}$$

From the equation above, we can calculate the loss resistance of a lumped inductor and include it into our antenna model. As we can see from Fig. 3.13, the major losses are caused by dielectric loss and conductivity loss. The loss caused by the two lumped inductors is minor.

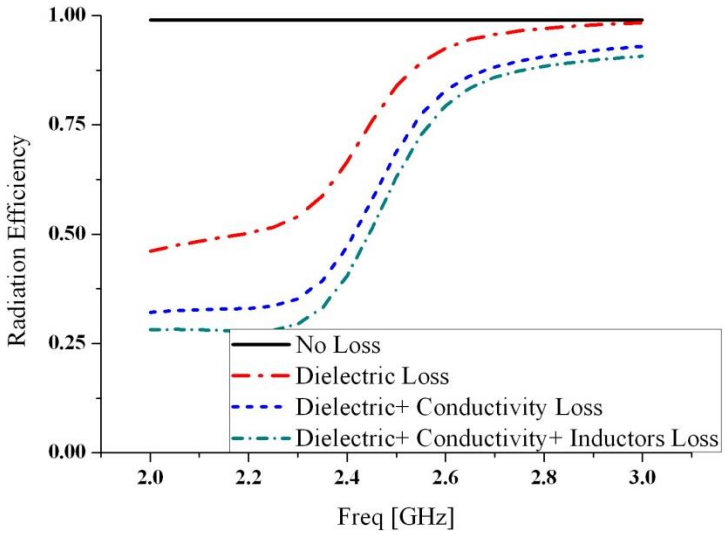

Fig. 3.13. Radiation efficiency

3.3 Simulation Results of Designed Antenna with the Presence of Human Head Model

3.3.1 Simplifications of the Numerical Human Head Model

The human head model used in this section was developed by Aarkid (a 3D modeling company), supplied by HFSS [29] which is shown in Fig. 3.14. The model includes the whole human body consisting of most of the human body organs which can be imported separately. The electromagnetic properties of a human organ at a certain frequency can be found in [30-31]. It has been verified though that the part below the shoulder will not affect the simulation results significantly at this range of frequency, since hearing aid devices are inserted around ears, which is more than three

wavelengths away from the shoulders. Thus, the human body model below the shoulder has been removed to improve the simulation efficiency.

It has been observed in the course of the simulations that more simplifications can be applied to the head model. It has been noticed that the results remain almost the same when only the essential parts, brain, skull, eyes and skin, are kept and all other detail parts are replaced by a homogeneous material. By using the simplified head model, the simulation time would be almost 7 times faster compared to the complete head model.

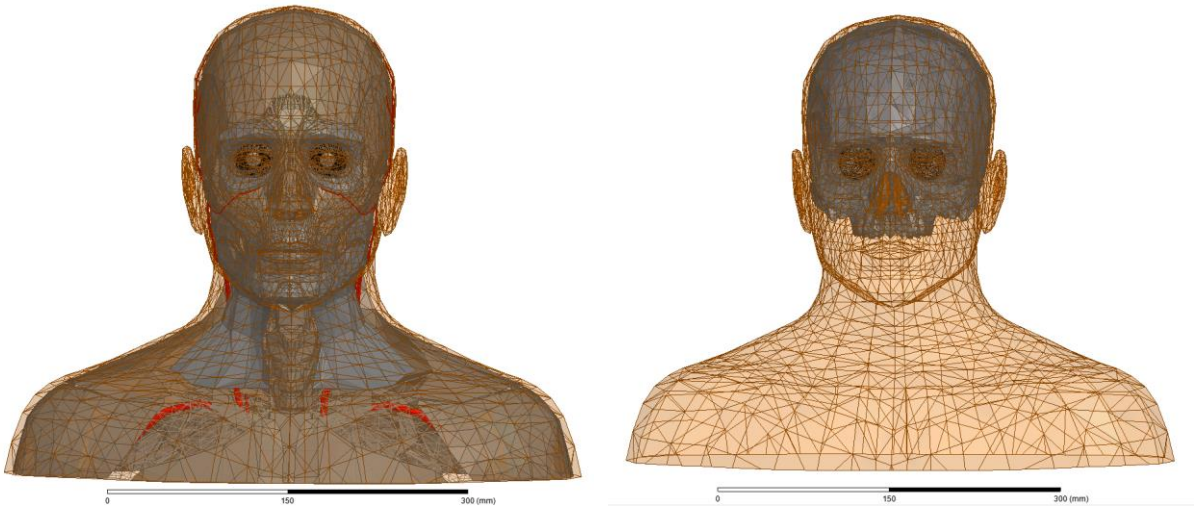

(a) (b)

Fig. 3.14. Numerical human head model: (a) Complete model; (b) Simplified model

3.3.2 Comparisons of Simulation Results between Complete Head Model and Simplified Model

The configuration, consisting two hearing aid devices in HFSS is shown in Fig. 3.15(a). The two hearing aid devices, which are inserted around ears, wirelessly communicate with each other. Due to the asymmetry of the antenna, which exists between the left and the right traces, the input impedance of the antenna around the left ear (antenna 1) may be different from the one inserted around the right ear (antenna 2). This discrepancy between the two antennas is not desired since the objective here is to design one type of hearing aid device for both of the ears. This asymmetry is improved by the two

lumped components implanted on the antenna structure. By varying the values of lumped components, the differences between the two antennas can be minimized.

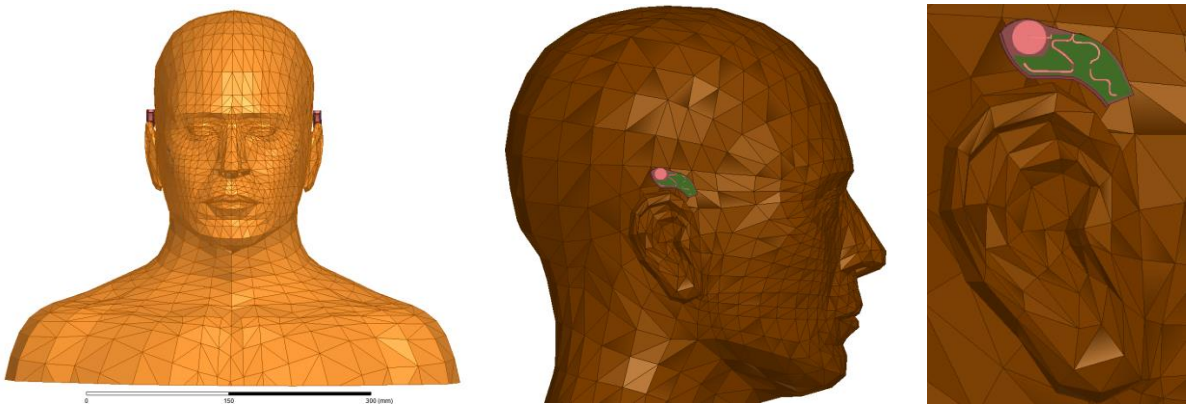

(a) (b) (c)

Fig. 3.15. Antenna with the presence of head model: (a) Configuration of the hearing aid system; (b) Side view around right ear; (c) Zoomed in around right ear

As mentioned in section 3.2, the optimized values of the two inductors, L1 and L2, are 3.6nH and 0.1nH respectively. With these optimized values, we can get well matched impedances on both antennas and good insertion loss between two antennas as we will see later.

As we mentioned before, the human head model has been simplified in such a way to achieve similar results compared to the complete head model, with respect to the differential return loss, S(d1d1) and S(d2d2), and the differential insertion loss, S(d1d2) and S(d2d1). All the differential return loss and insertion loss can be derived from section 2.1 using the transformation between standard scattering matrix and mixed-mode scattering matrix. Since the whole hearing aid antenna system is passive and lossless, we know that S(d1d2) and S(d2d1) are identical according to reciprocity theorem. Thus, we take S(d2d1) as the insertion loss between left ear and right ear antennas for the following study.

As observed from Fig. 3.16(a), using the simplified head model, the return loss for antenna 1 or antenna 2 is almost the same with that of the complete human head model. Only the local geometry around human ear plays the dominant role on the antenna impedance. The return loss of both antennas are below -10dB, which means good matching has been accomplished.

The insertion loss between antenna 1 and 2 for both simplified and complete head model is demonstrated in Fig. 3.16 (b). Small variations are observed in the insertion loss as the frequency goes above 2.7 GHz. But at our desired band (2.4GHz- 2.5GHz), S(d2d1) is almost identical for the simplified and the complete head model. According to the results shown in Fig. 3.16, the replacement of the complete head model by the simplified head model is not only efficient, but also does not cause any significant error at desired frequency band in our simulations. Therefore, from now on the simplified human head model has been utilized for further analysis and designs. And at 2.4GHz-2.5GHz frequency band, the insertion loss is around -70dB. Since the transmitter output power of this hearing aid device is 4dBm and the receiver sensitivity is -93dBm, the insertion loss observed from our simulation will be good enough for this application.

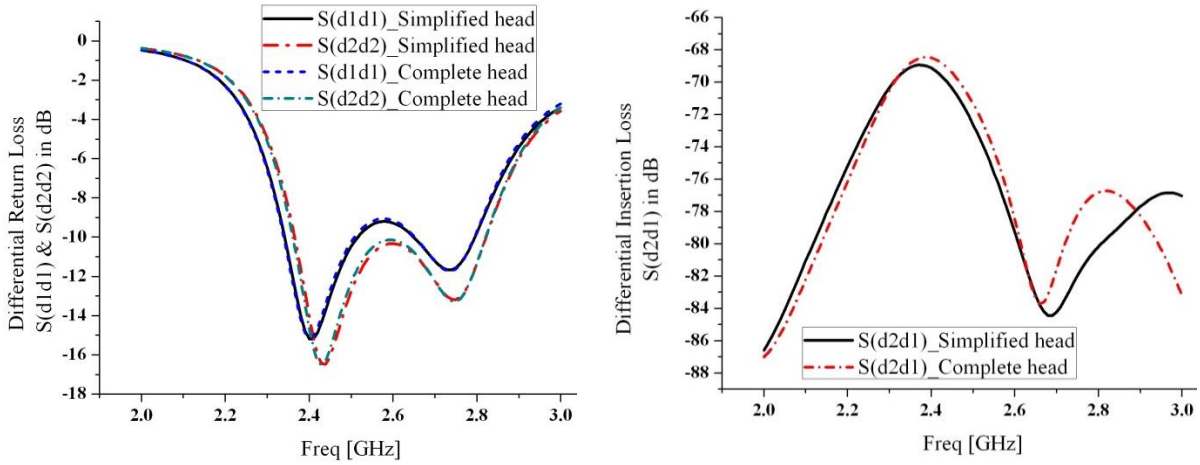

(a) (b)

Fig. 3.16. Comparisons between complete model and simplified model: (a) Differential return loss S(d1d1) & S(d2d2); (b) Differential insertion loss S(d2d1)

The plots of the electric field and magnetic field of a cross-section in the direction of the wave propagation at 2.4GHz, 2.45GHz and 2.5GHz using simplified human head model are demonstrated in Fig. 3.17. The E-field decays rapidly inside the human head since human head acts as highly lossy material at this range of frequency, which can also be proved by taking a careful look at the wavelength inside the head and around head. The head attenuates the H-field minimally if any at all, because of the non-magnetic property of the human head. Both surface wave propagating around head

and directed wave propagating inside head exist at this range of frequency for ear-to-ear communication. And it is difficult to tell which one of them takes the dominant role. It will depend on the certain operating frequency and placements of the transmitter and receiver.

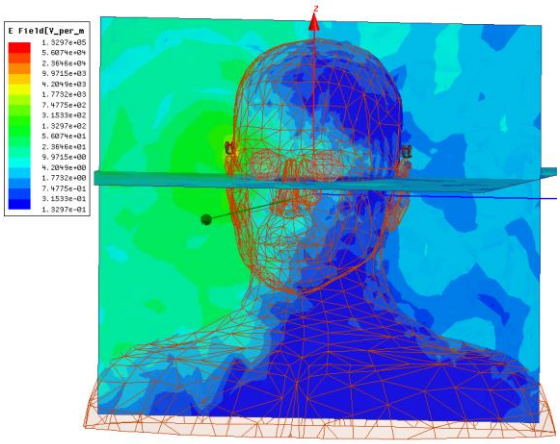

(a)

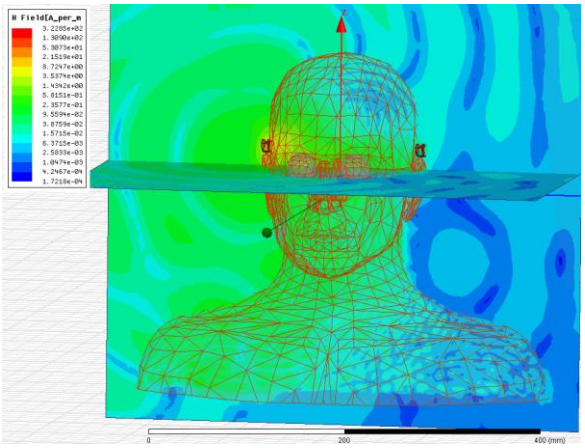

(b)

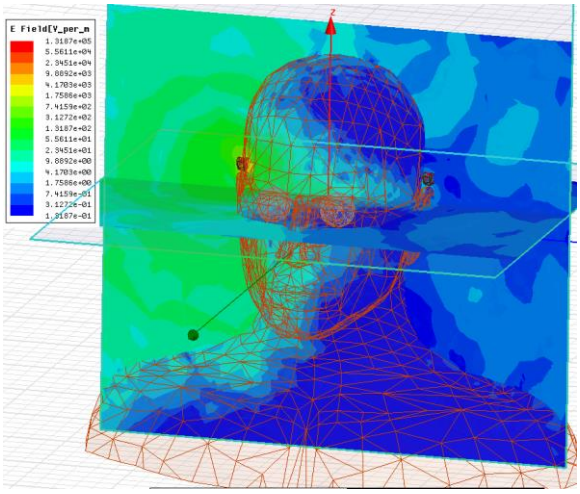

(c)

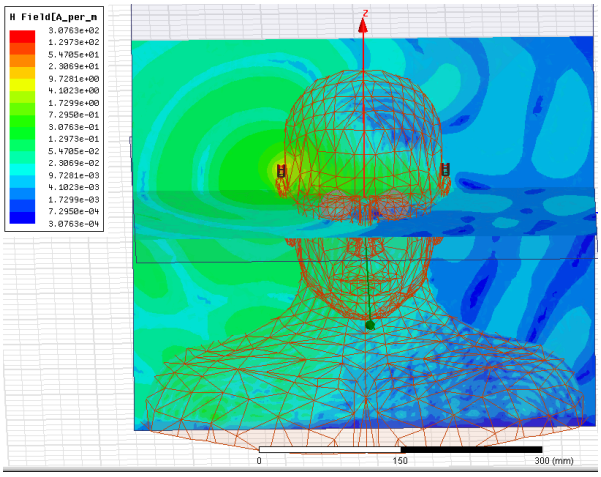

(d)

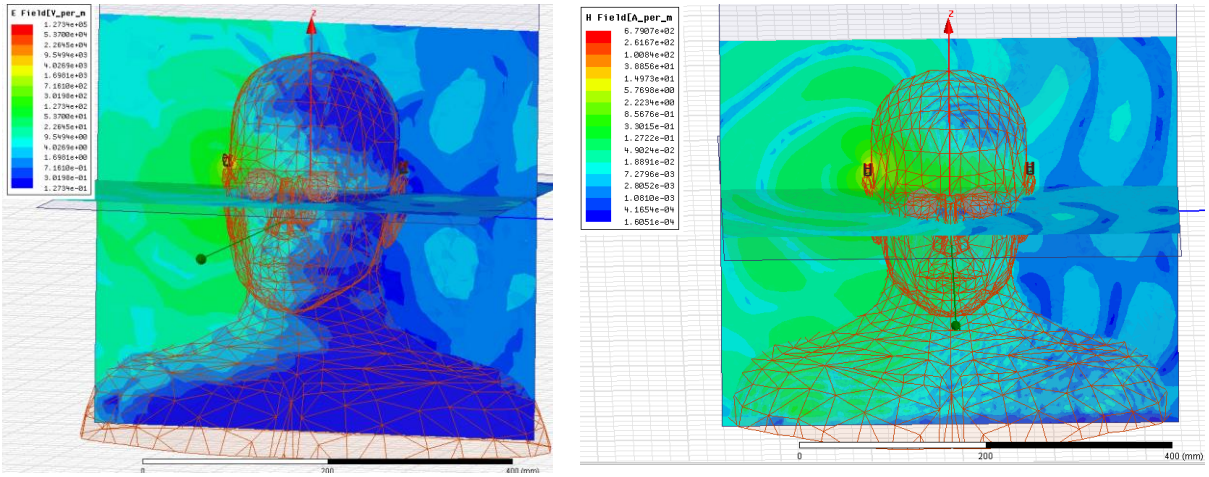

(e) (f)

Fig. 3.17. Field inside and around simplified human head model: (a) E-field at 2.4GHz; (b) H-field at 2.4GHz; (c) E-field at 2.45GHz; (d) H-field at 2.45GHz; (c) E-field at 2.5GHz; (d) H-field at 2.5GHz

3.3.3 Parameter Study of Simplified Human Head Model

In order to investigate whether the antenna works well for different size of the human head or not, we scale the size of the head model to 0.9 times and 1.1 times compare to original model, respectively. For simplification, we name these three models as small, medium and large head model. As demonstrated in Fig. 3.18(a), the differences between the return loss of both antennas (1 and 2) for these three models are tolerated. However, the changes of insertion loss through the whole band (2-3GHz) are unpredictable as shown in Fig. 3.18(b). But at the desired band, the insertion loss goes down as the size of the head increases as expected. Generally speaking, hearing aid devices using the designed antenna can be utilized by people with different head size.

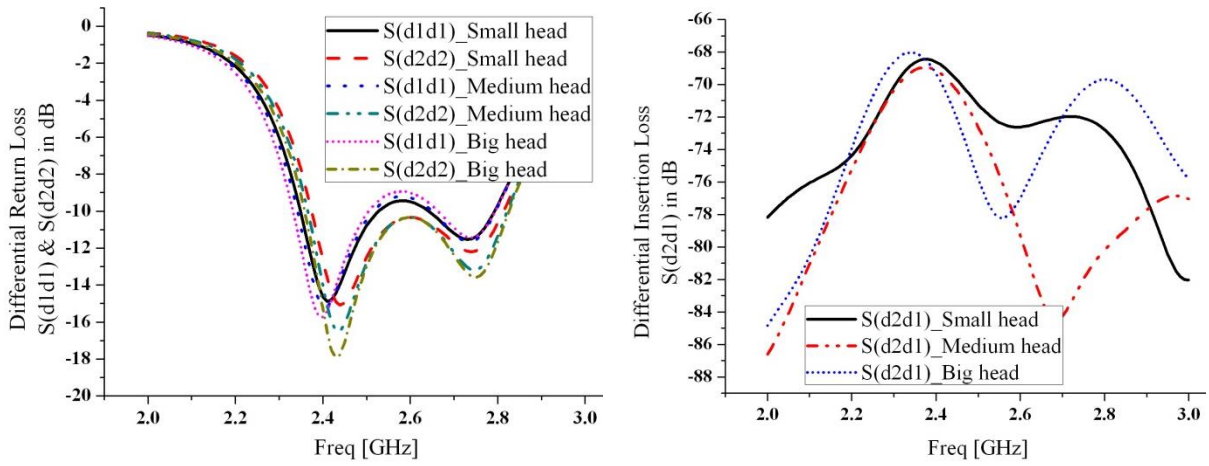

(a) (b)

Fig. 3.18. Effects of head size on: (a) Differential return loss S(d1d1) & S(d2d2); (b) Differential insertion loss S(d2d1)

Another thing we want to study is how the return loss and the insertion loss change when we make some changes on the electromagnetic properties (permittivity and conductivity) of the remained organs (skin and brain). So we can know whether this simplified head model works for different kinds of people since there may be some changes on the electromagnetic properties (permittivity and conductivity) of the skin and brain of different people. For this purpose, we increase/decrease the permittivity/conductivity of the skin and brain by 10 percent of their original values respectively and compare the results with the original simplified head model. The results are as follows.

From Fig. 3.19, we can see that the changes on the permittivity or conductivity on the skin won't change the return loss of the antennas much. The local geometry of human ear dominates on the antenna impedance instead of small changes on the electromagnetic properties of human skin. And the changes on insertion loss are within 2dB at desired band (2.4GHz- 2.5GHz) as shown in Fig. 3.20.

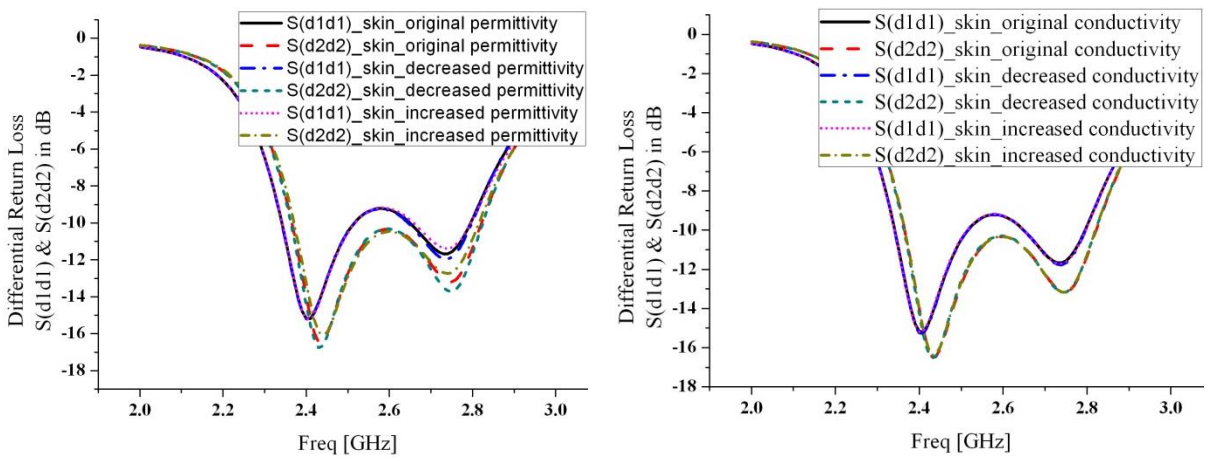

(a) (b)

Fig. 3.19. Effects on the differential return loss S(d1d1) and S(d2d2) when we make changes on: (a) Permittivity of skin; (b) Conductivity of skin

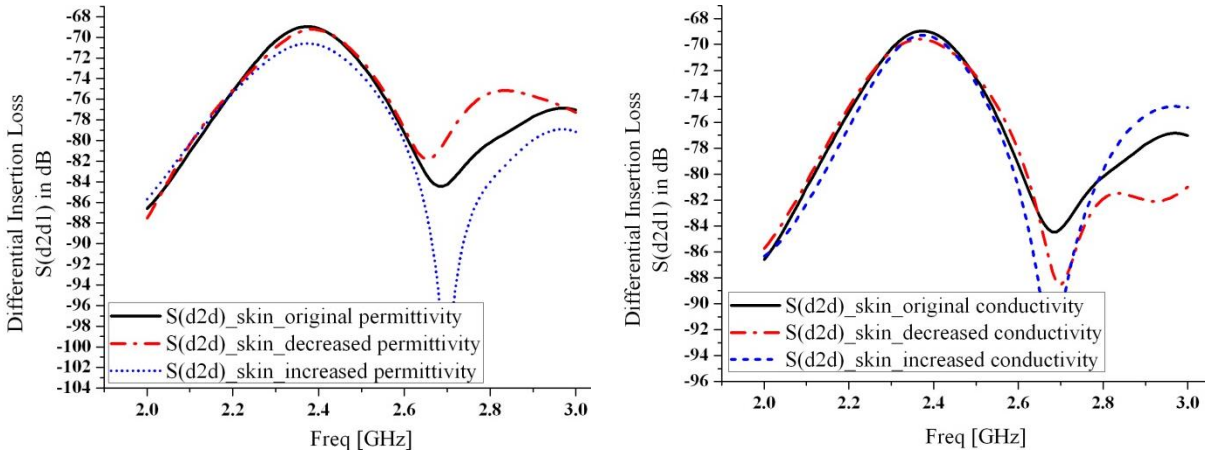

(a) (b)

Fig. 3.20. Effects on the differential insertion loss S(d2d1) when we make changes on: (a) Permittivity of skin; (b) Conductivity of skin

From Fig. 3.21, we can conclude that the changes on the permittivity or conductivity on the brain won't change the return loss of the antennas much. And the changes on insertion loss are within 2dB at desired band (2.4GHz- 2.5GHz) as shown in Fig. 3.22.

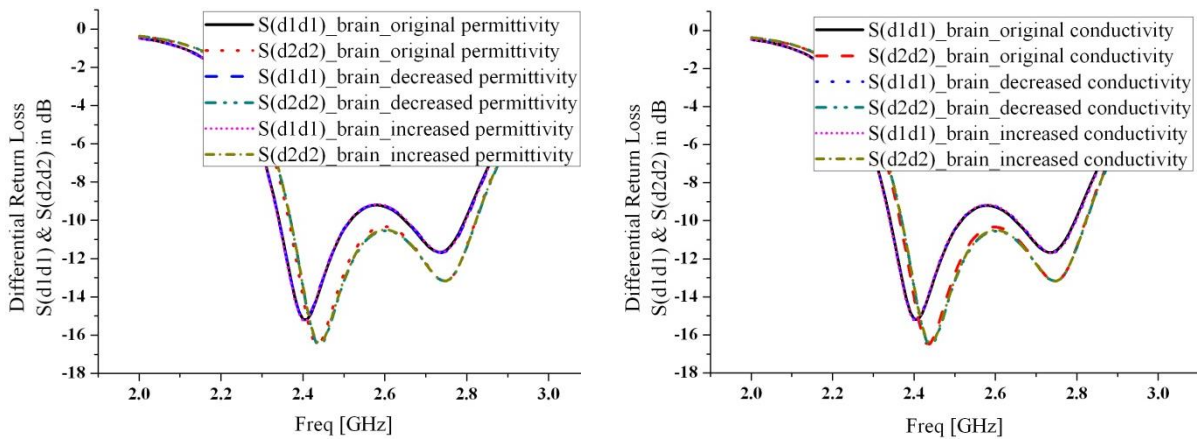

(a) (b)

Fig. 3.21. Effects on differential return loss S(d1d1) and S(d2d2) when we make changes on: (a) Permittivity of brain; (b) Conductivity of brain

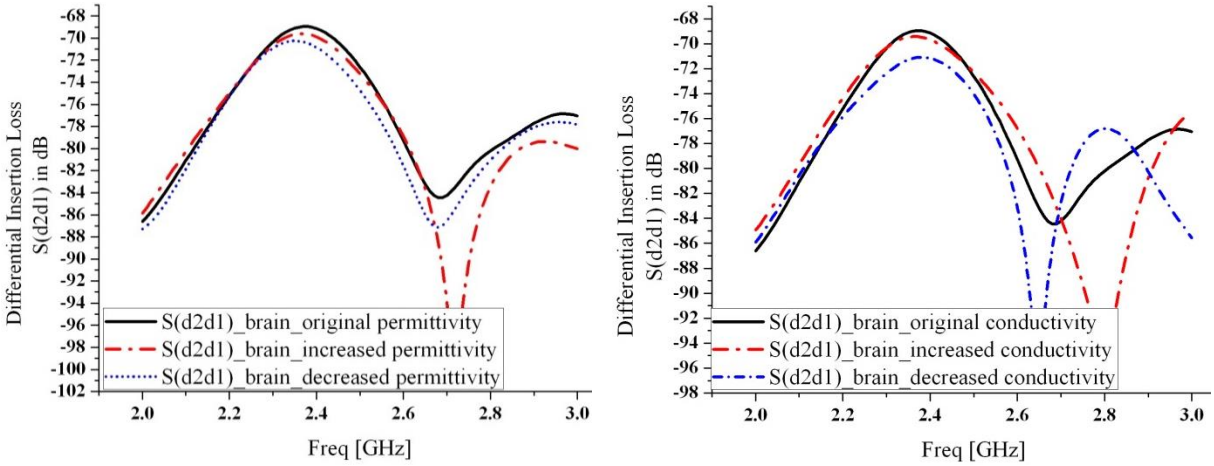

(a) (b)

Fig. 3.22. Effects on differential insertion loss S(d2d1) when we make changes on: (a) Permittivity of brain; (b) Conductivity of brain

From the parameter study of the simplified human head model on return loss and insertion loss in this part, we can conclude that designed antenna works well for different human heads. Maybe the antenna performance is different when different people wear it, but we can always optimize its

performance by adjusting the two lumped inductors implanted on the antenna structure. And as we will discuss in chapter four, these two lumped elements can also be lumped capacitors.

3.4 Measurement of Designed Antenna

3.4.1 Fabricated Antenna Samples and Measurement Setup

Designed antenna was fabricated and some samples are shown in Fig. 3.23. The substrate used in this sample was flexible material UL3850 with a thickness of 0.1mm, provided by Rogers Corporation, as we mentioned in section 3.2. The antenna arms and ground were made of copper with a cladding of 0.5 oz. The width of the antenna arm trace was 0.5mm, which was the same width as the 0402 planar lumped component.

As shown in Fig. 3.23(a), except the expected discontinuity at the center of each antenna arm, two extra discontinuities close to the start and the end of each antenna arm were implemented for possible needs of implanting extra lumped components or simply changing the location of lumped components for the sake of impedance matching. The extra discontinuity part was soldered together when not used as the location for the implanting a lumped component. Between the two arms, there was the common ground for differential signals.

While we folded the planar structure of fabricated sample into the three-dimensional model designed before, foam was used to keep the separation of two planes of the arms of the designed antenna to be 5mm. SMA cables were used for testing as we can see from the two test antenna samples shown in Fig. 3.23(b). For one test sample, we needed two identical SMA cables to make sure that designed antenna was excited by balanced differential signals coming from radio at the input ports of the antenna. The center conductors of the two SMA cables were soldered to the starting points of two arms of the antenna respectively. The shields of the two cables were soldered together to the antenna ground. One more thing needs to be pointed out is that a Balun, which was a copper cylinder with a length of 3cm (a quarter wavelength at 2.45GHz), was connected to the cable shields to prevent possible radiation caused by SMA cables.

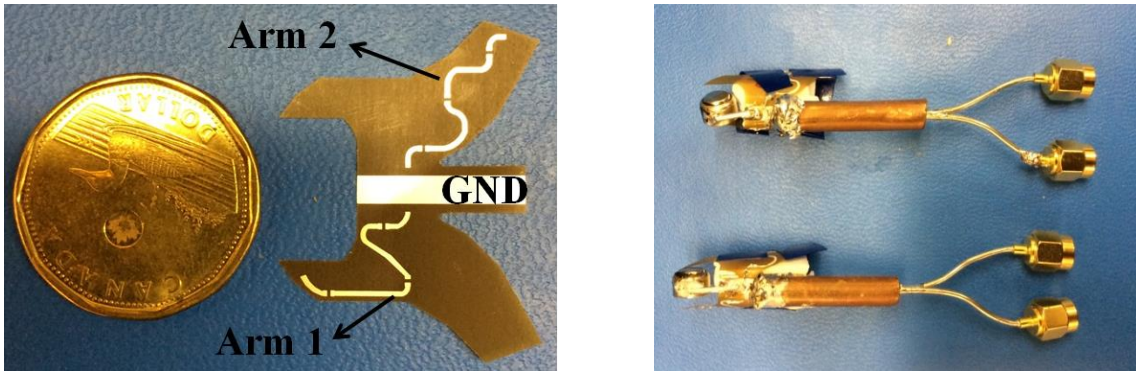

(a) (b)

Fig. 3.23. Fabricated antenna samples: (a) Planar structure; (b) Two test samples with SMA cables

Vector network analyzer (VNA) is needed to measure the antenna impedance. But for a normal VNA, it cannot generate differential signal and measure differential impedance directly. So a Balun board designed by a CIARS lab engineer Shadi Dashmiz, as shown in Fig. 3.24, was used to generate differential signals to excite the designed differential dipole antenna. The input port, which is connected to a VNA under testing, is port 1 in the Fig. 3.24. The two output ports, which are connected to the two SMA cables of a test sample, are port 2 and 3 respectively.

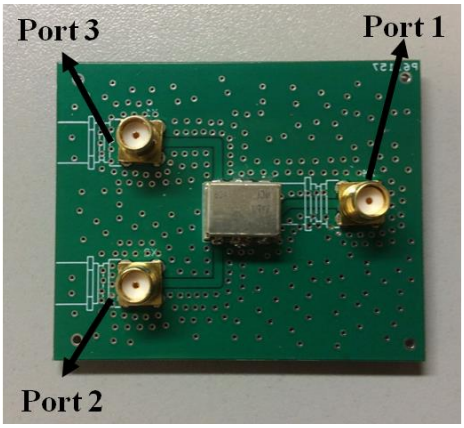

Fig. 3.24. A Balun board designed to generate differential signals

The scattering parameters of this Balun board were tested and the results are shown in Fig. 3.25. From Fig. 3.25(a), we can see that the S(1,1) is below -10dB from 2GHz to 2.7GHz which means

majority of power is delivered to the two output ports. The power from port 1 is equally divided to port 2 and port 3 as shown in Fig. 3.25(b). And the phase difference between port 2 and port 3 is constantly 180 degree. In summary, this Balun board can generate very good differential signals that can be used to excite the designed differential dipole antenna.

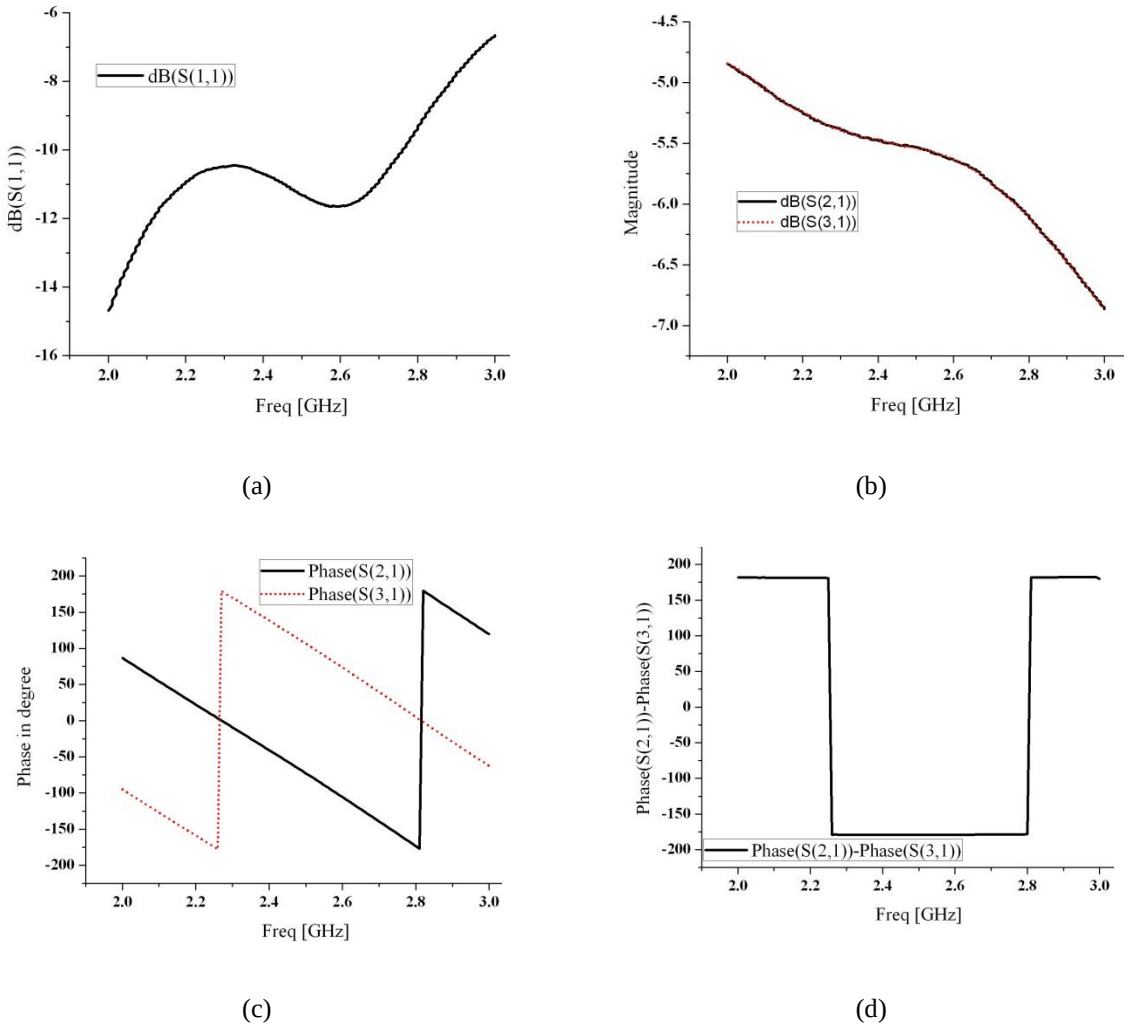

Fig. 3.25. Scattering parameters of the Balun board: (a) Magnitude of S(1,1) in dB; (b) Magnitude of S(2,1) and S(3,1) in dB; (c) Phase of S(2,1) and S(3,1) in degree; (d) Phase difference between S(2,1) and S(3,1) in degree

The block diagram of measurement setup is shown in Fig. 3.26(a). A VNA, which was used to generate a signal at desired frequency band, was connected to the input port (port 1) of the Balun board mentioned before. The single-ended signal was transferred into balanced differential signals by

the Balun board and delivered to the two output ports. Each output port was connected to one of the two identical SMA cables, and then the antenna was excited by the differential signals coming from the SMA cables. After we got the one-port scattering matrix at the input of the Balun board (which was the reference plane for a VNA to measure scattering matrix), we needed to de-embed the effects of the Balun board and SMA cables to get the actual antenna impedance. The methods used to de-embed the effects of the Balun board and SMA cables can be found in [32-35]. After de-embedding, the reference planes was moved to the excitation planes of the differential antenna (which were also the ends of the SMA cables) and we can get the standard two-port scattering matrix. Then we can use the transformation between standard scattering parameters and mixed-mode scattering parameters mentioned in chapter 2 to compute the differential return loss or differential impedance we need.

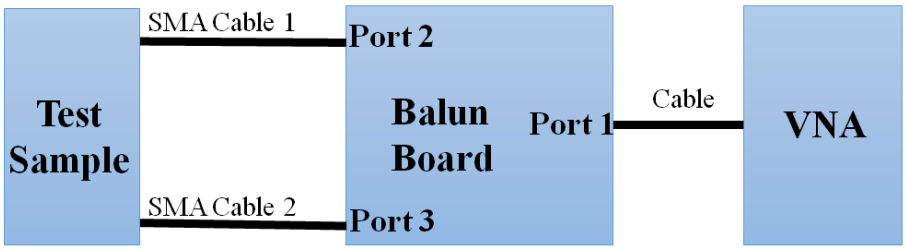

(a)

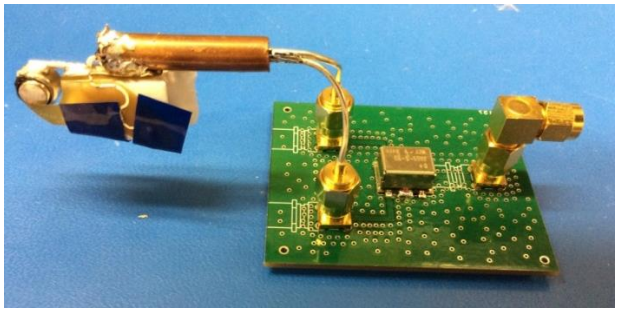

(b)

Fig. 3.26. Measurement setup: (a) Block diagram; (b) A test sample with the Balun board

Although we can move the reference planes to the ends of the SMA cables by de-embedding and get the two-port scattering matrix, there were still some remaining effects of the SMA cables since the

current on the cable shields may cause some radiation. To make all the comparisons between simulations and measurements in the following parts as accurate as possible, we included the SMA cables with the same lengths and radiuses of center conductor and shield conductor as the actual antenna sample used in the test and re-modelled the antenna. From now on, all the simulation results are based on the new model shown in Fig. 3.27. The antenna was excited by two plane waves with the same amplitude and 180 degree phase difference at the starts of the cables.

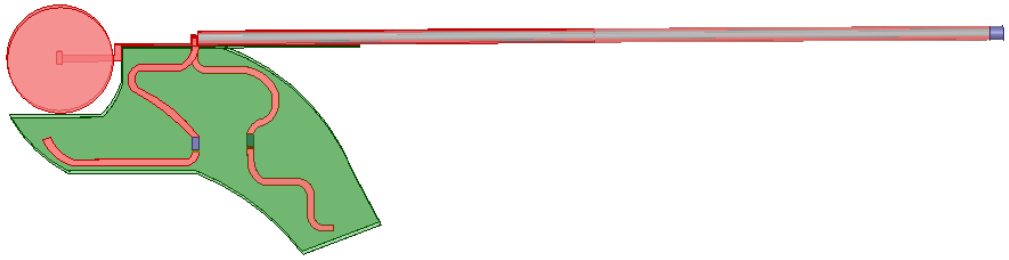

Fig. 3.27. New antenna model including cables

3.4.2 Measurement Results in Free Space

To study the amount of undesired radiation caused by SMA cables compared to the amount of desired radiation generated by antenna arms, we plot the current distribution on the antenna arms and cables in the free space environment as shown in Fig. 3.28. From the zoomed in current distribution around the antenna arms and the starts of the cables, we can tell that the current on the shields of the cables are at least 10 times weaker than the current on the antenna arms and the center conductors of the cables, which means the amount of undesired radiation caused by SMA cables is much weaker than the amount of desired radiation generated by antenna arms.

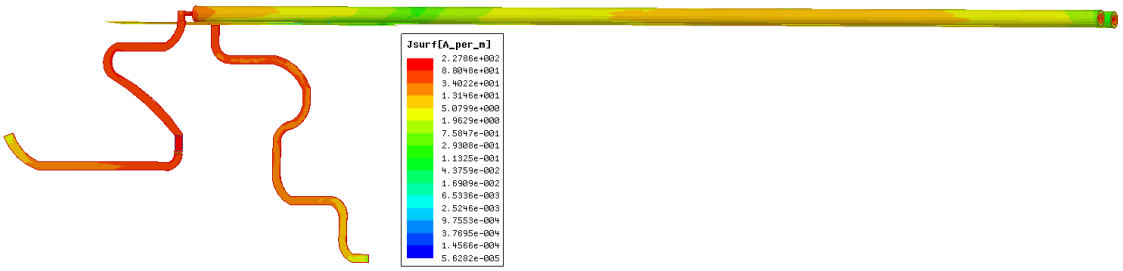

(a)

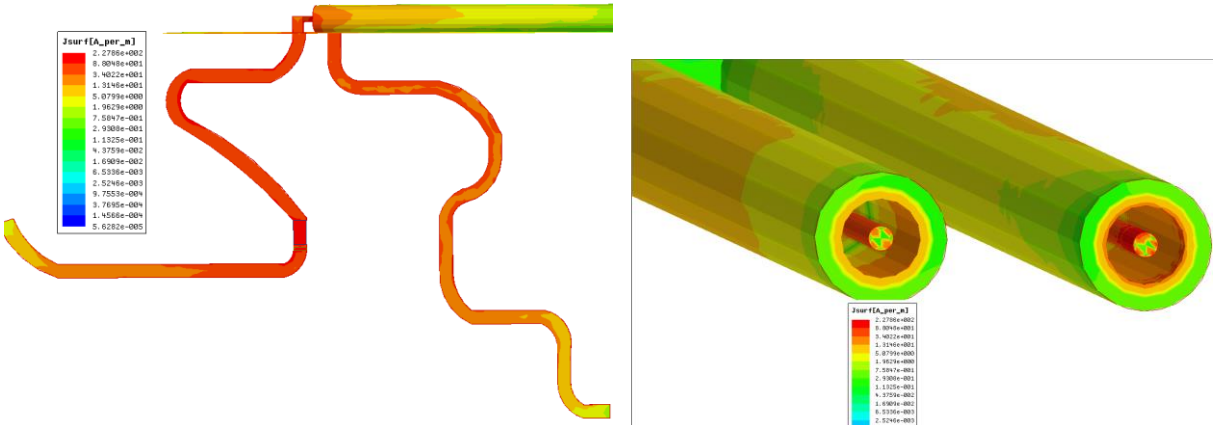

(b) (c)

Fig. 3.28. Current distribution on the antenna arms and cables: (a) Overall distribution; (b) Zoomed in around antenna arms; (c) Zoomed in around the starts of cables

To minimize the interferences from the test environment, the test sample was surrounded by absorbers as shown in Fig. 3.29. One can either choose to move the whole measurement setup inside an anechoic chamber and cover the VNA with absorbers to minimize the scattering waves caused by the big metal piece (VNA), or do the test at a lab environment and surround the test antenna sample with absorbers. Since the test sample is much smaller compared to a VNA, we chose the second method and surrounded the sample with thick absorbers to get high accuracy measurement data.

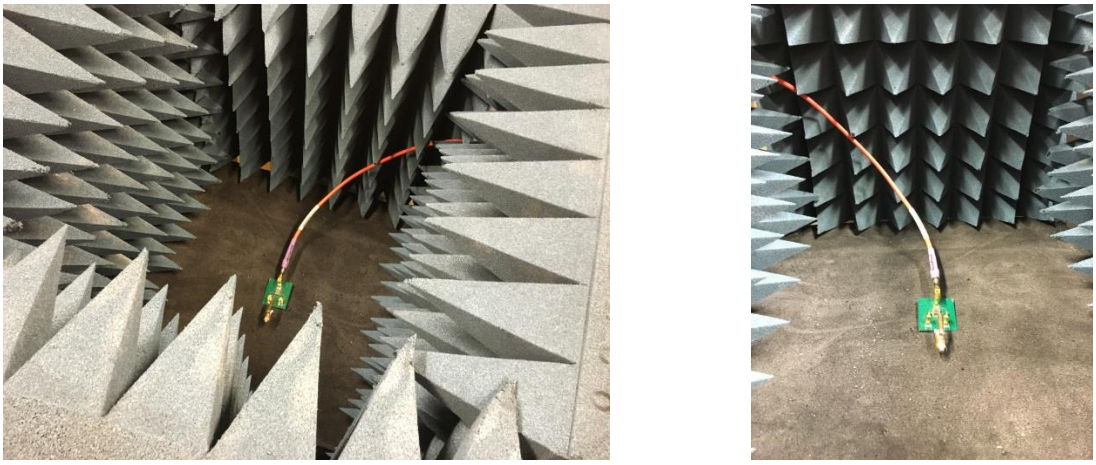

(a) (b)

Fig. 3.29. Measurement setup in free space: (a) Overall view; (b) Close view around test sample

The comparisons of standard two-port scattering parameters between simulations of the new antenna model and measurements of two samples are shown in Fig. 3.30 and Fig. 3.31.

From Fig. 3.30, we can conclude that the resonant frequencies of S(1,1), S(2,1) and S(2,2) of sample 1 are all shifted to higher bands compared to that of the S(1,1), S(2,1) and S(2,2) of simulated model. Since the antenna is passive and lossless, the insertion loss S(2,1) and S(1,2) between the two excitation ports are identical. And we only plot S(2,1) here. But the overall trends of the both magnitudes and phase of the standard two-port scattering parameters between simulated model and sample 1 are the same. These discrepancies could be caused by the deviations in the processing of building the test sample 1.

A better agreement of the magnitudes of the standard two-port scattering parameters between simulated model and sample 2 is observed from Fig. 3.31(a). Magnitudes of simulated and measured S(1,1) and S(2,2) are almost overlapped. And in terms of the magnitudes of S(2,1), there is only a nearly constant deviation between simulation and measurement. But we must note that there are shifts to higher bands in terms of the phases as shown in Fig. 3.31(b), and these shifts are understandable since the phase measurements are more likely affected by the errors caused in the processing of

building test sample and the interferences from the test environment. But in general, the differences between simulated antenna model and test samples are at acceptable ranges.

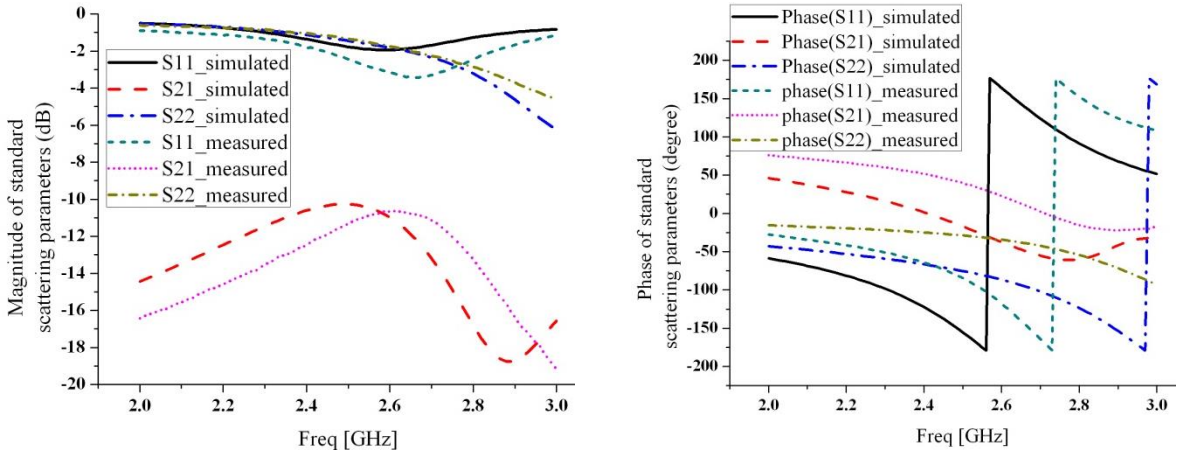

(a) (b)

Fig. 3.30. Comparisons of standard two-port scattering matrix between simulated model and test sample 1: (a) Magnitude in dB; (b) Phase in degree

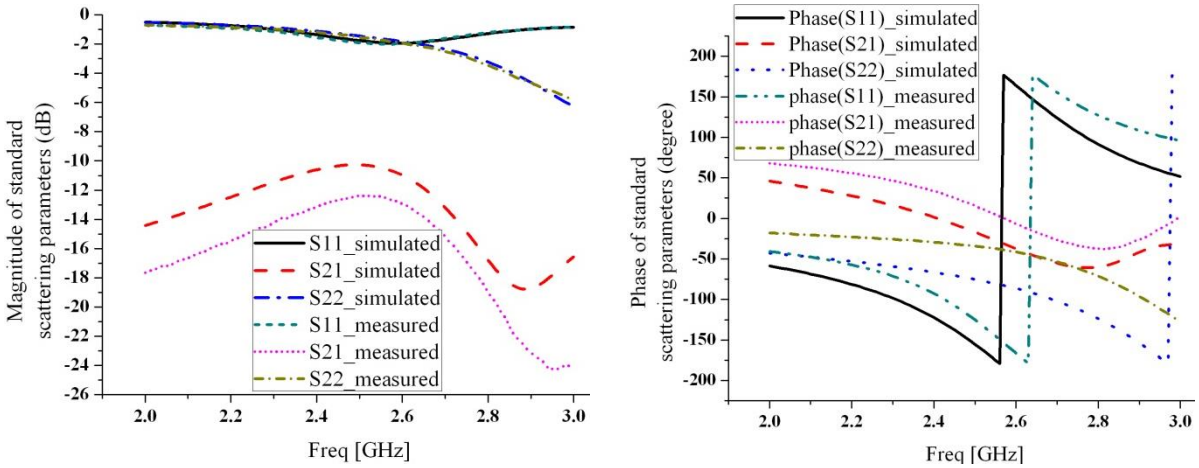

(a) (b)

Fig. 3.31. Comparisons of standard two-port scattering matrix between simulated model and test sample 2: (a) Magnitude in dB; (b) Phase in degree

Now, let's apply the transformation between standard scattering parameters and mixed-mode scattering parameters illustrated in chapter 2 to get the differential impedance at the input of the antenna. After converting the two-port standard scattering parameters into one-port mixed-mode scattering parameters, we got the differential return loss and differential impedance of this dipole antenna as shown in Fig. 3.32. As we expected, the differential return loss of sample 1 is shifted to higher frequency band compared to simulation as agreed with the shifts on the two-port standard scattering parameters demonstrated in Fig. 3.30. Small shifts on resonant frequencies between sample 2 and simulated model are also observed and they are due to the shifts on the phases between simulation and measurement. Both magnitudes and phases measurements are important in a differential test since the transformation between standard scattering parameters and mixed-mode scattering parameters needs both magnitude and phase information. And from Fig. 3.32(b), we can tell that the trends of both real and imaginary parts of the differential impedance are the same between simulated model and measured samples.

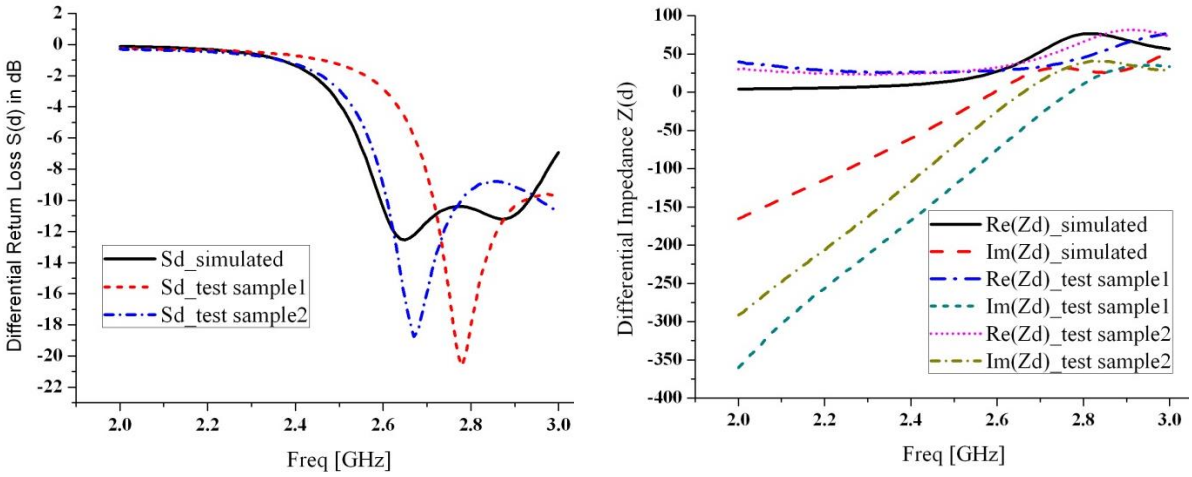

(a) (b)

Fig. 3.32. Differential parameters: (a) Differential return loss S(d) in dB; (b) Differential impedance Z(d) in ohm

From the measurement results of two antenna samples in the free space environment, we can conclude that the measurements done with sample 2 have better agreements with the simulated model. So for the differential impedance measurements with the presence of Specific

Antropomorphic (SAM) head model and actual human being head, we use sample 2 to do all the measurements.

3.4.3 Measurement Results with the Presence of SAM Head Model

Specific Antropomorphic (SAM) head model is a homogeneous head model which is widely used in the cellphone tests. There are two layers for a SAM head model, shield layer made of plastic material and inside layer filled by a liquid. The SAM head model used here for impedance measurement is provided by On Semiconductor and can work well at 2GHz- 3GHz frequency band. A numerical SAM head model developed by Ansys is used in the HFSS simulation. As we can see from Fig. 3.33, the simulated differential insertion loss S(d2d1) between two hearing aid antennas using SAM head model is at least 6dB higher than that using the complex head model mentioned in section 3.3. And the trends using these two different head models are not the same at the desired band. Usually, SAM head model is good for modelling antenna impedance for BAN application, but it's not good for modelling the insertion loss between two antennas for ear-to-ear communication application here.

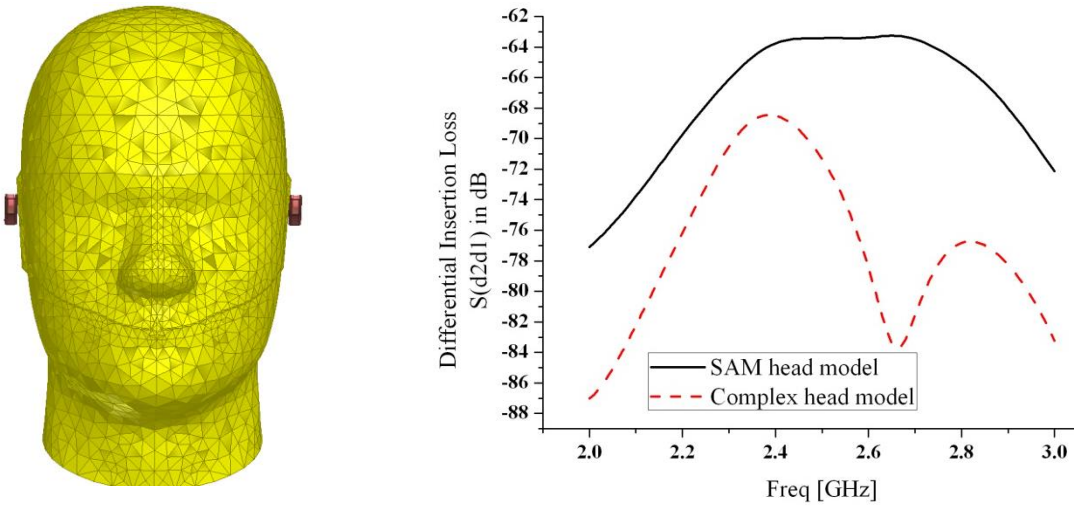

(a) (b)

Fig. 3.33. (a) Hearing aid system using SAM head model; (b) Differential insertion loss between two antennas

Because of the asymmetrical structure of this dipole antenna, the differential impedance of the antenna could be different when we put the antenna close to the left ear or right ear of SAM head

model. From now on, for a test, putting antenna close to the left ear and right ear of SAM head model or real human being head are called left ear scenario and right ear scenario, respectively. The simulation and measurement setups for both left ear scenario and right ear scenario are shown in Fig. 3.34 and Fig. 3.35. For the measurements, both test antenna sample and SAM head model were surrounded by thick absorbers.

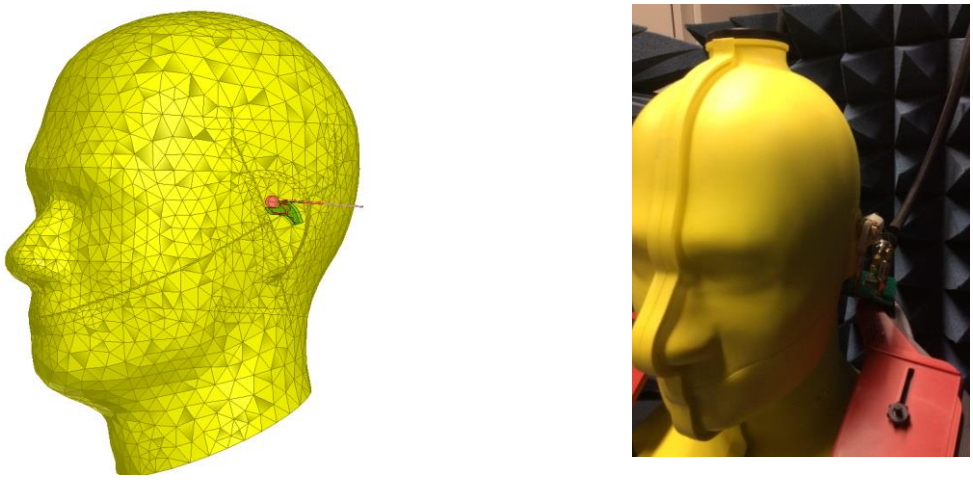

(a) (b)

Fig. 3.34. Left ear scenario: (a) Simulation setup; (b) Measurement setup

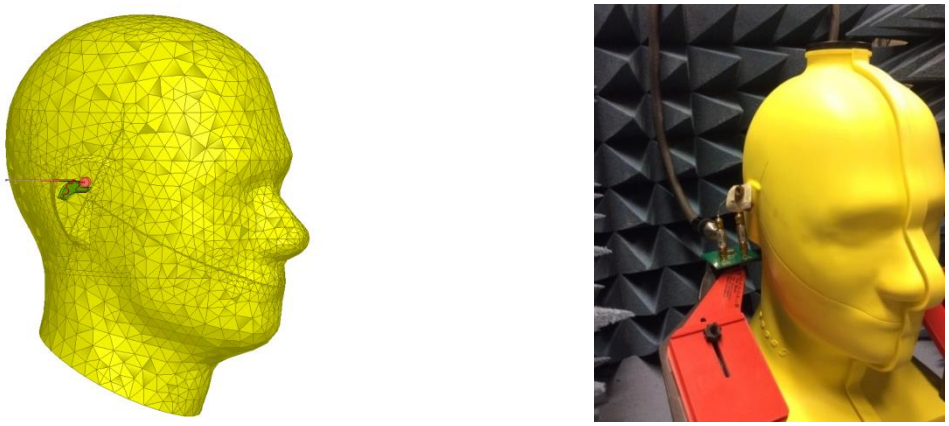

(a) (b)

Fig. 3.35. Right ear scenario: (a) Simulation setup; (b) Measurement setup

The comparisons of differential return loss between simulation and measurement are demonstrated in Fig. 3.36. For the left ear scenario, a good agreement is observed between simulation and measurement. And a down-shift on the resonant frequency is observed for the right ear scenario. But the overall trends for both scenarios between simulations and measurements are the same, which means the designed antenna can work properly with the presence of SAM head model.

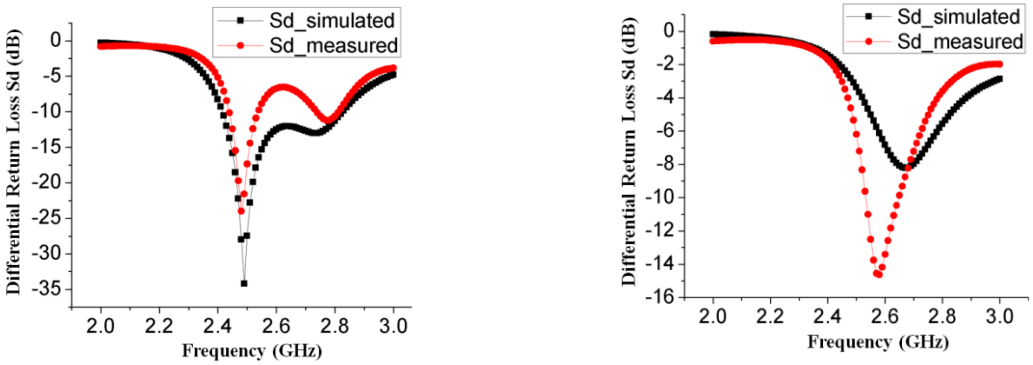

(a) (b)

Fig. 3.36. Comparisons of differential return loss S(d) between simulation and measurement: (a) Left ear scenario; (b) Right ear scenario

3.4.4 Measurement Results with the Presence of Actual Human Being Heads

Matching the antenna impedance to the radio with the presence of an actual human being head is the most difficult part of this research since every human being has a different head. The complex head model or simplified model presented in section 3.3 can work for parts of human beings and give us a good starting point for our design including the human body effect. There is not one human body model that is good for modeling every person anyway. But for our proposed antenna, we can always re-match the antenna to the desired impedance by changing the lumped elements loaded on the antenna structure as long as the mismatch is within acceptable range.

To study the changes on the antenna impedance at different locations of a real human being head, we measured the antenna impedance at two different positions on the same person's head for both left ear scenario and right ear scenario. The results are shown in Fig. 3.37. As we can see, the resonant frequency would shift unpredictably when the relative location of test antenna is changed with the

respect to the human ear for both left ear scenario and right ear scenario. The antenna impedance really depends on the local geometry of the location where the antenna is put on.

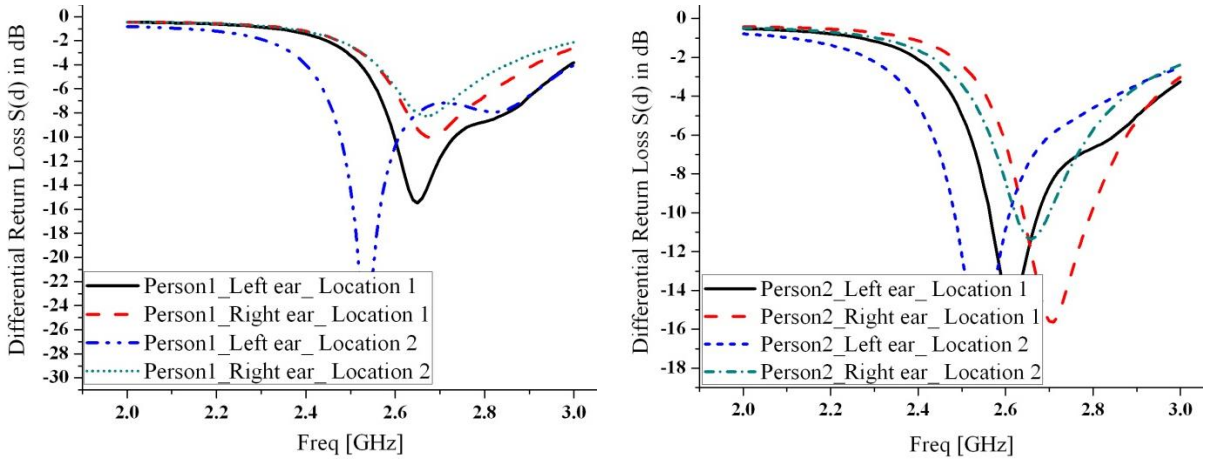

(a) (b)

Fig. 3.37. Differential return loss S(d) at different locations of human heads: (a) Person 1; (b) Person 2

To study the changes on the antenna impedance for different human beings, we measured the differential return loss of the antenna for six more persons as shown in Fig. 3.38. Again, the resonant frequency would be different for each person. But the resonances are all in the range of 2.3GHz and 2.7GHz. We can retune the antenna for an individual by changing the lumped elements loaded on the antenna. We must state that the measurements done in this section are not repeatable because the measurements highly depend on the test environment and people who participate in the test. But the impedance measurements with the presence of actual human beings done in this section are still good to show that the designed antenna can work with real human beings.

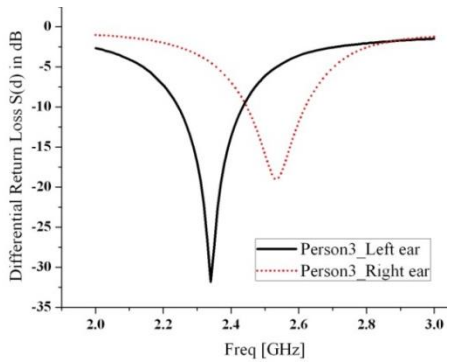

(a)

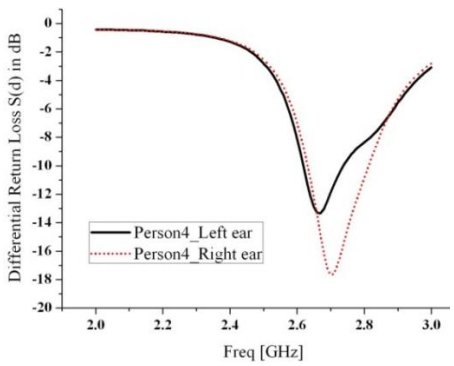

(b)

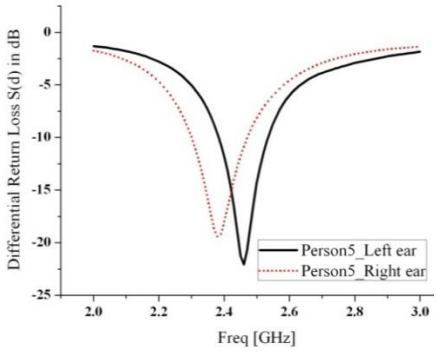

(c)

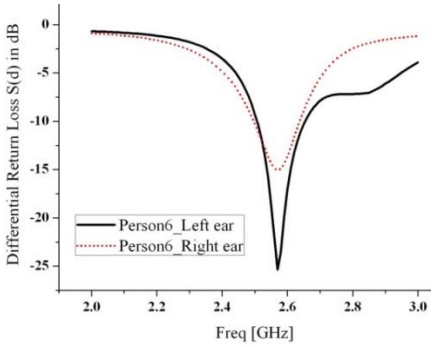

(d)

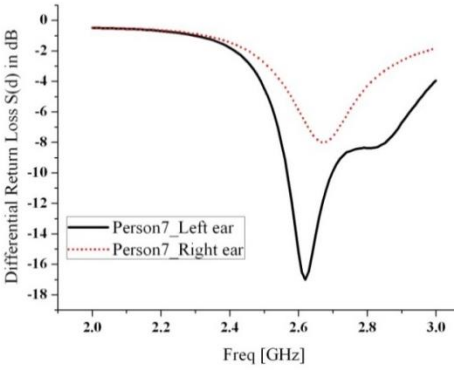

(e)

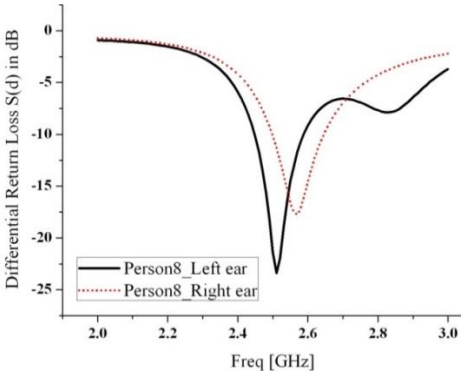

(f)

Fig. 3.38. Differential return loss S(d) for different persons: (a) Person 3; (b) Person 4; (c) Person 5; (d) Person 6; (e) Person 7; (f) Person 8

In summary, a lumped inductors loaded differential dipole antenna was designed. The simulation and measurement results of designed antenna were demonstrated in this chapter and the results showed that the designed antenna would be a promising choice for Bluetooth enabled hearing aid devices.

Chapter 4. Integration of a Lumped Capacitors Loaded Dipole Antenna with a Hearing Aid Package

4.1 Design of a Lumped Capacitors Loaded Differential Dipole Antenna

A lumped capacitors loaded dipole antenna was designed to be fitted into a specific hearing aid package focusing on ear-to-remote communication application. Good radio link was observed between transmitting hearing aid device and receiving cellphone after integrating the designed antenna with a hearing aid radio board package, and vice versa.

Compared to the dipole antenna designed in chapter three, the available PCB space for this antenna was decreased to half the size as before as shown in Fig. 4.1. A differential dipole antenna with symmetrical arms was designed for this finalized PCB. Same as before, the two antenna arms were separated by the ground, which was connected to the battery. Two lumped capacitors C1 and C2, instead of inductors, were implanted at the center of the antenna arms. The reason behind this choice was that we wanted to investigate whether integrating tunable elements, for example voltage controlled capacitors, on the antenna structure to achieve adaptive matching for different human heads was doable or not.

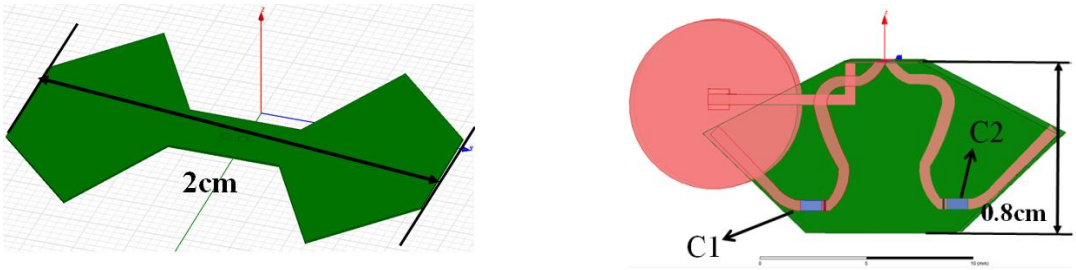

(a) (b)

Fig. 4.1. A lumped capacitors loaded dipole antenna: (a) Available PCB size for antenna; (b) Designed antenna model

The tunable capacitors designed by STMicroelectronics with a package of 0.65*1.0*0.3mm can be used for this application [36]. The available values of these tunable capacitors operating from DC to

3GHz are: 1.2pF, 2.7pF, 3.3pF, 3.9pF, 4.7pF, 5.6pF, 6.8pF, and 8.2pF. These tunable capacitances are controlled through a bias voltage ranging from 2 to 20 volts. And the tuning range C_{2V}/C_{20V} is 3.5, which means that, for a specific tunable capacitor, the capacitance can be changed consistently from its highest value to 2/7 of its highest value. We can change the resonant frequency of the designed antenna by changing the values of C1 and C2 manually as shown in Fig. 4.2. For this stage, we haven't been able to integrate the tunable capacitors directly on the antenna structure. But the idea of tuning the antenna by tunable capacitors is doable. Achieving adaptive matching by integrating voltage controlled capacitors on the antenna structure for miniaturized device operating at BAN could be a valuable future work for this research.

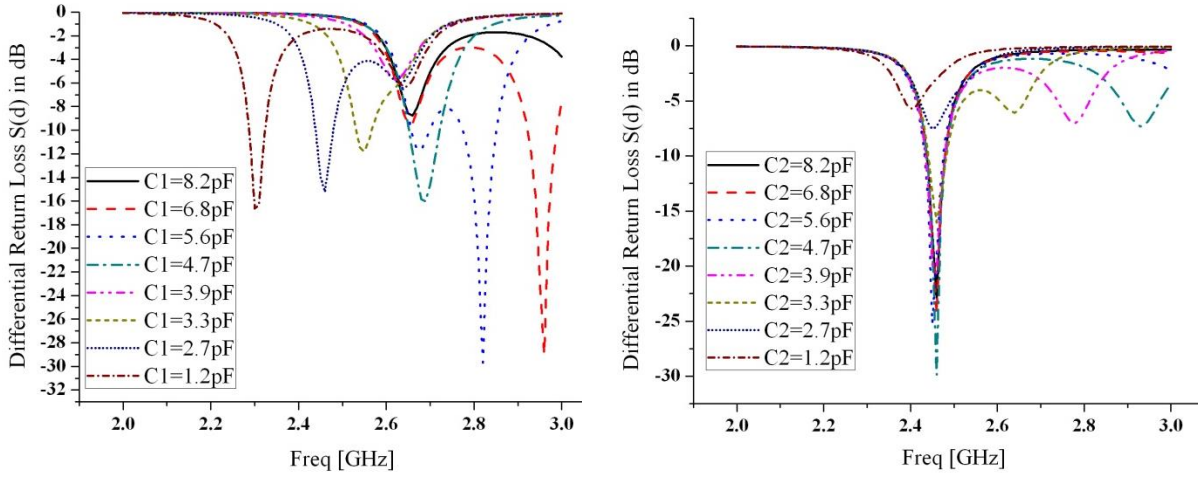

(a) (b)

Fig. 4.2. Resonant frequency VS capacitances: (a) Varying C1; (b) Varying C2

4.2 Integration of Designed Antenna with a Hearing Aid Radio Board Package

A radio board designed by On Semiconductor was used for the hearing aid device and the impedance of radio input/output is 22-j32 ohms. To enable the maximum power transfer, the antenna impedance with the presence of head needed to be conjugate matched to the radio. The simplified head model mentioned in section 3.3 was used to optimize the antenna impedance to 22+j32 ohms. Since this hearing aid device focused on ear-to-remote communication application, we only needed to optimize the antenna impedance to the desired value for both left ear scenario and right ear without worrying

about the insertion loss between two ears. By setting the capacitances of the two lumped capacitors implanted on the antenna arms to be 3.3 pF and 2.7pF respectively, the antenna impedance was nearly conjugate matched to the radio for both left ear and right ear scenarios as shown in Table 1.

Table 1. Impedance table

Radio input/output impedance	Antenna impedance: Free space	Antenna impedance: Left ear scenario	Antenna impedance: Right ear scenario
22-j32 ohms	19-j26 ohms	18+j34 ohms	23+j30 ohms

The designed antenna was fabricated and a sample is shown in Fig. 4.3(a). Since the antenna ground in the simulation model was actually the RF ground of the radio board and the antenna arms were identical, there was no need to fabricate the antenna using a flexible material anymore. We fabricated the antenna using the low cost FR4 substrate with a thickness of 0.4mm, same as simulation, and then connected the two arms directly to the differential radio input/output without cables as shown in Fig. 4.3(b). Then we fitted the radio board and antenna into a small hearing aid case and assembled the rest parts as well. A fully assembled hearing aid device is shown in Fig. 4.3(d) and the size of the device is comparable to a coin.

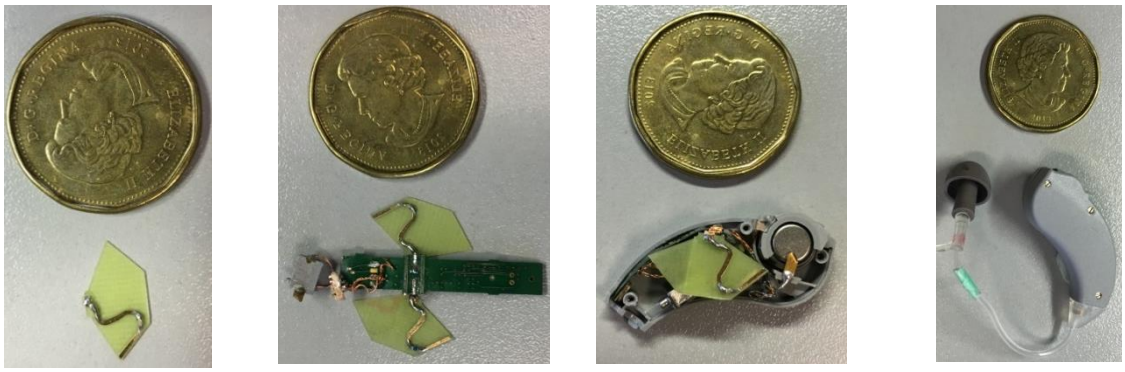

(a) (b) (c) (d)

Fig. 4.3. A hearing aid device: (a) Antenna sample; (b) Integration of antenna with a radio board; (c) Fitting antenna and radio board into a case; (d) Fully assembled device

4.3 Link Tests between Hearing Aid Device and Cellphone

To evaluate the antenna performance after integration with the other parts, some link tests were done and the results are presented in this section. For the ear-to-remote communication application here, the objective was to have a good link between transmitter and receiver within 10m range at all the directions at an indoor environment. For link tests, a cellphone with 2.4GHz- 2.5GHz Bluetooth band antenna and a hearing aid device were needed. The hearing aid device needed to work well at both transmitting mode and receiving mode, so two sets of link tests were done. The transmitting power was always 4dBm no matter it was the hearing aid device or the cellphone working at the transmitting mode, and the receiver sensitivity was always -93dBm no matter which one was the receiver.

Firstly, the hearing aid device was working at transmitting mode (the transmitter) and the cellphone was the receiver. A measurement setup is shown in Fig. 4.4 and the measurements were done inside a small anechoic chamber. The hearing aid device attached to the left ear or right ear of the SAM head model kept sending constant power of 4dBm at the output of its radio, and the cellphone located one foot away from the hearing aid device kept recording the received power at the input of its LNA. For each test, the cellphone stored the measured power within a time span of five minutes as shown in Fig. 4.5. As we can see, the received power by the cellphone was stable after two minutes and then we took the average value of the last three minutes as the power received by the cellphone. To compare the performances of the designed lumped capacitors loaded dipole antenna with another antenna (here we call it ITIS antenna) provided by another partner of ON Semiconductor which was also designed for this hearing aid device, we used the same measurement setup for ITIS antenna. From Fig. 4.5, we can tell that the capacitors loaded antenna works well for both left ear scenario and right ear scenario, but the ITIS antenna only works well for right ear scenario. For the capacitors loaded antenna, since the average received power by cellphone was no less than -53dBm with a separation of one feet from the transmitter, the radio link range can easily go beyond 10m for both left ear scenario and right ear scenario, which means the designed antenna worked well with the presence of the SAM head model.

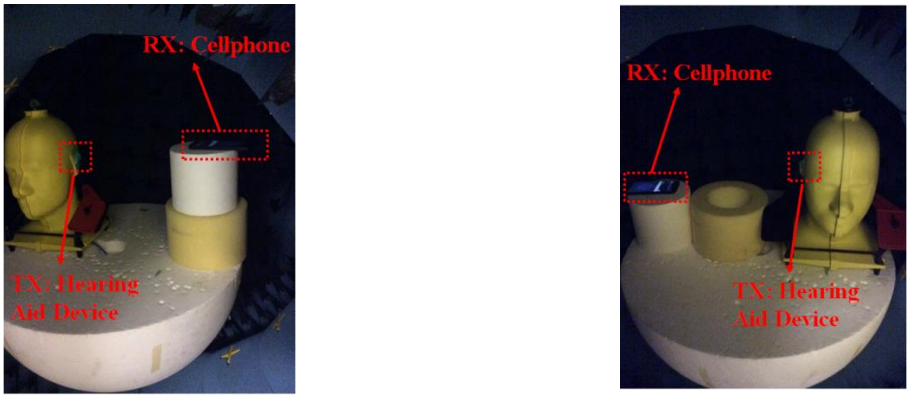

(a) (b)

Fig. 4.4. Radio link tests inside a small anechoic chamber: (a) Left ear scenario; (b) Right ear scenario

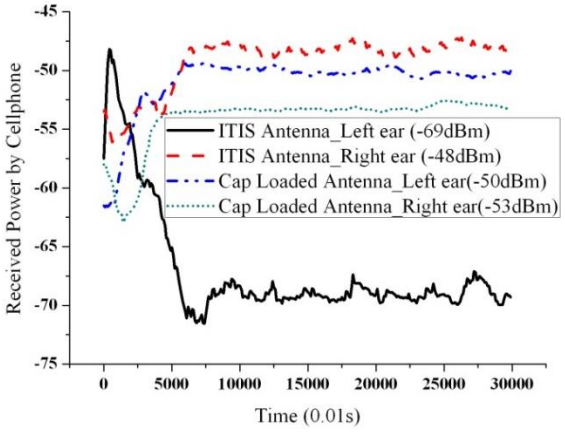

Fig. 4.5. Received power by cellphone with the presence of the SAM head model

Then, some radio link range tests were done with actual human beings at indoor (office) environment. As shown in Fig. 4.6, we tested the link ranges at four different directions, which are called as facing the same ear case (For example, if the transmitter, hearing aid device is on the left ear of a person as shown in Fig. 4.6(a), then the case that the receiver cellphone located at the left side of a person is called facing the same ear case), facing the opposite ear case, facing the nose case and facing the back case for both left ear scenario and right ear scenario of a person. The tests were done for two persons.

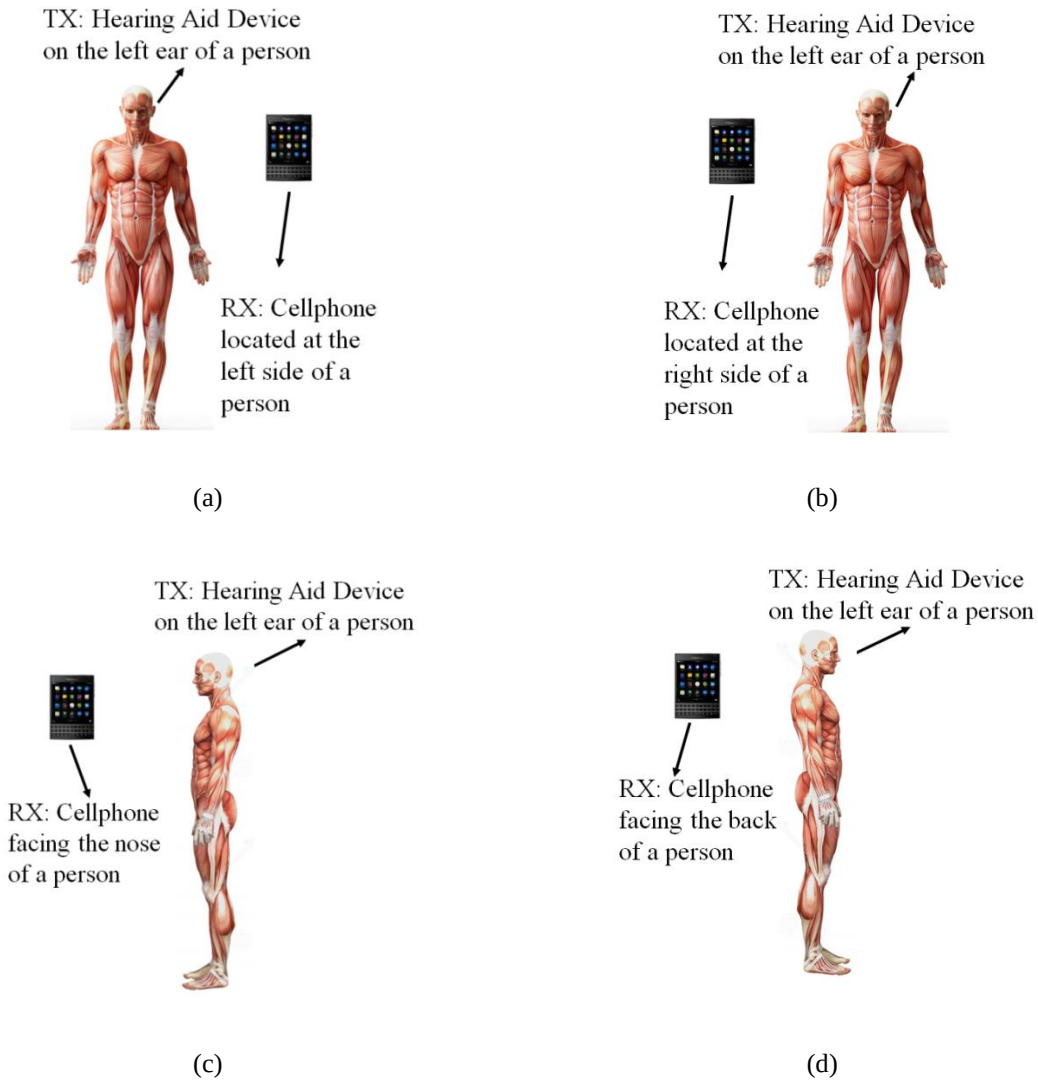

Fig. 4.6. Measurement setup illustration: (a) RX facing the same ear case; (b) RX facing the opposite ear case; (c) RX facing the nose case; (d) RX facing the back case

The results of the radio link range tests are demonstrated in Table 2. As we can see, for the two persons, the radio link ranges at all the four directions were beyond 10m for both left ear scenario and right ear scenario. And as we expected, the radio link ranges for facing the opposite ear case were the worst. This was because that most of the directed waves from hearing aid device towards the cellphone direction were attenuated by the highly lossy human head. But since there were scattering waves from ceiling, ground and other objects of the room, the radio link range can still go about 10m.

Table 2. Radio link range (m): TX was the hearing aid device and RX was the cellphone

Radio link range (m)	RX facing the same ear case	RX facing the opposite ear case	RX facing the nose case	RX facing the back case
TX on the left ear of person 1	21	11	17	13
TX on the right ear of person 1	18	10	16	15
TX on the left ear of person 2	19	10	15	16
TX on the right ear of person 2	20	10	17	15

Lastly, the audio link range tests at the same office environment were done when the cellphone was working at the transmitting mode and the hearing aid device was working at the receiving mode. The hearing aid device attached to the left ear or right ear of a person kept receiving the audio from the cellphone. As we mentioned before, the output power of the cellphone was still 4dBm and the receiver sensitivity of the hearing aid device was still -93dBm. Same as the radio link range tests mentioned before, the audio link range tests were done with the same two persons for both left ear scenario and right scenario. The results of audio link range tests are shown in Table 3. As we can see, the audio link ranges were clearly worse than the radio link ranges done before. This was because that the audio link range tests required the hearing aid device was able to receive a power that was always more than -93dBm, otherwise the link between cellphone and hearing aid device would be terminated immediately. But for the radio link range tests, the link between hearing aid device and cellphone wouldn't be terminated immediately even if the received power by cellphone were below -93dBm. The received power by cellphone could go up than -93dBm and the radio link range would be further. But except the facing the opposite ear direction, the audio link ranges can go beyond 10m at all the other three directions. And the good thing is that we can increase the transmitting power of the

cellphone without worrying about affecting one's health as it is not the one which is always on a person's head.

Table 3. Audio link range (m): TX was the cellphone and RX was the hearing aid device

Audio link test (m)	TX facing the same ear case	TX facing the opposite ear case	TX facing the nose case	TX facing the back case
RX on the left ear of person 1	14	7	10	10
RX on the right ear of person 1	13	6	11	11
RX on the left ear of person 2	13	7	9	11
RX on the right ear of person 2	13	7	10	10

In summary, a lumped capacitors loaded differential dipole antenna was designed to meet specific ear-to-remote communication applications. And results of the link range tests showed that the antenna works well after integrating with the radio board package, which means designed antenna is good for real products.

Chapter 5. Conclusion and Future Work

In conclusion, this thesis proposed a novel lumped elements loaded differential dipole antenna for blue-tooth enabled hearing aid devices. Miniaturization and direct matching were realized by implanting lumped components on the antenna structure. Proposed antennas were simulated, fabricated and measured. The measurements had good agreements with simulations. And for body area network applications, human body model can be simplified according to specific application to shorten time in the antenna design. Further, the designed antenna worked well after integrating with a radio board package for a hearing aid device focusing on ear-to-remote communication application.

As mentioned in this thesis, the effects of human body on the impedance of an antenna operating in/on or around the body area network are unpredictable for different human beings. So integrating tunable elements, for example voltage controlled capacitors, directly on the antenna structure to achieve adaptive matching according to different human body will be a valuable future work for this research.

Bibliography

[1] Poslad, S., “Ubiquitous Computing Smart Devices, Smart Environments and Smart Interaction”. *Wiley*, 2009.

[2] Schmidt, R., Norgall, T., Bernhard, J., “Body Area Network BAN- a key infrastructure element for patient-centered medical applications”. *Biomed Tech* 47: 365-8, 2002.

[3] O’Donovan, T., O’Donoghue, J., Sreenan, C., Sammon, D., “A Context Aware Wireless Body Area Network (BAN)”. In proceeding of the Pervasive Health Conference 2009.

[4] Yuce, M.R., “Implementation of wireless body area networks for healthcare systems”. *Sensors and Actuators A: Physical* 162: 162-129, Jun 2010.

[5] Yuce, M.R., Khan, J.Y., “Wireless Body Area Networks: Technology, Implementation, and Application”. *Pan Stanford Publishing*, Dec 2011.

[6] http://www.google.ca.

[7] http://ihcrp.georgetown.edu/agingsociety/pdfs/hearing.pdf.

[8] Shaker, G.S.A.; Nezhad-Ahmadi, Mohammad-Reza; Safavi-Naeini, S.; Weale, G., "On design of a low power wireless hearing aid communication system," in *Microwave Symposium Digest, 2008 IEEE MTT-S International* , vol., no., pp.903-906, 15-20 June 2008.

[9] Shaker, G.; Nezhad-Ahmadi, M.-R.; Safavi-Naeini, Safieddin; Weale, G., "Modeling and design of a wireless hearing aid communication system," in *Radio and Wireless Symposium, 2009. RWS '09. IEEE*, vol., no., pp.127-130, 18-22 Jan. 2009.

[10] Moore, D.R., “Anatomy and physiology of binaural hearing”. International Journal of Audiology, vol.30, Issue 3, pp.125-134, 1991.

[11] Zhichao Li; Shaker, G.; Nezhad-Ahmadi, M.-R.; Safavi-Naeini, S., "Design of a miniaturized antenna for Bluetooth-enabled hearing aid devices," in *Antennas and Propagation & USNC/URSI National Radio Science Meeting, 2015 IEEE International Symposium on* , vol., no., pp.772-773, 19-24 July 2015.

[12] Chandra, R.; Johansson, A.J., "Miniaturized antennas for link between binaural hearing aids," in *Engineering in Medicine and Biology Society (EMBC), 2010 Annual International Conference of the IEEE* , vol., no., pp.688-691, Aug. 31 2010-Sept. 4 2010.

[13] Jaehoon Kim; Rahmat-Samii, Y., "An implanted antenna in the spherical human head: SAR and communication link performance," in *Wireless Communication Technology, 2003. IEEE Topical Conference on*, vol., no., pp.202-203, 15-17 Oct. 2003.

[14] Koulouridis, S.; Nikita, K.S., "Study of the coupling between human head and cellular phone helical antennas," in *Electromagnetic Compatibility, IEEE Transactions on* , vol.46, no.1, pp.62-70, Feb. 2004.

[15] Conway, G.A.; Scanlon, W.G., "Antennas for Over-Body-Surface Communication at 2.45 GHz," in *Antennas and Propagation, IEEE Transactions on* , vol.57, no.4, pp.844-855, April 2009.

[16] Kvist, S.H.; Ozden, S.; Thaysen, J.; Jakobsen, K.B., "Improvement of the ear-to-ear path gain at 2.45 GHz using parasitic antenna element," in *Antennas and Propagation (EUCAP), 2012 6th European Conference on* , vol., no., pp.944-947, 26-30 March 2012.

[17] Kvist, S.H.; Thaysen, J.; Jakobsen, K.B., "Polarization of unbalanced antennas for ear-to-ear on-body communications at 2.45 GHz," in *Antennas and Propagation Conference (LAPC), 2011 Loughborough* , vol., no., pp.1-4, 14-15 Nov. 2011.

[18] Kellomaki, T.; Whittow, W.G.; Heikkinen, J.; Kettunen, L., "2.4 GHz plaster antennas for health monitoring," in *Antennas and Propagation, 2009. EuCAP 2009. 3rd European Conference on*, vol., no., pp.211-215, 23-27 March 2009.

[19] Augustine, R.; Alves, T.; Zhadobov, M.; Poussot, B.; Sarrebourse, T.; Sauleau, R.; Thomas, M.K.; Laheurte, J.-M., "SAR reduction of wearable antennas using polymeric ferrite sheets," in *Antennas and Propagation (EuCAP), 2010 Proceedings of the Fourth European Conference on* , vol., no., pp.1-3, 12-16 April 2010.

[20] Kim, J.H.; Lee, H.M., "Low specific absorption rate wearable antenna for WLAN band applications," in *Antennas and Propagation (EuCAP), 2010 Proceedings of the Fourth European Conference on* , vol., no., pp.1-5, 12-16 April 2010.

[21] Kvist, S.H.; Thaysen, J.; Jakobsen, K.B., "Ear-to-ear on-body channel fading in the ISM-band for tangentially-polarized antennas," in *Antennas and Propagation Conference (LAPC), 2011 Loughborough*, vol., no., pp.1-4, 14-15 Nov. 2011.

[22] Nour, B.; Breinbjerg, O., "Measurement and characterization of the path loss for ear-to-ear wireless communication," in *Antennas and Propagation (EUCAP), Proceedings of the 5th European Conference on* , vol., no., pp.1621-1625, 11-15 April 2011.

[23] Kvist, S.H.; Thaysen, J.; Jakobsen, K.B., "Ear-to-Ear On-Body Channel Model for Hearing Aid Applications," in *Antennas and Propagation, IEEE Transactions on* , vol.63, no.1, pp.344-352, Jan. 2015.

[24] Kvist, S.H.; Thaysen, J.; Jakobsen, K.B., "Investigation of the ear-to-ear radio propagation channel," in *Antennas and Propagation (EUCAP), Proceedings of the 5th European Conference on* , vol., no., pp.3640-3644, 11-15 April 2011.

[25] Chandra, R.; Johansson, A.J., "Influence on the ear-to-ear link loss from heterogeneous head phantom variations," in *Antennas and Propagation (EUCAP), Proceedings of the 5th European Conference on* , vol., no., pp.1612-1615, 11-15 April 2011.

[26] Fan, W.; Lu, A.; Wai, L.L.; Lok, B.K., "Mixed-mode S-parameter characterization of differential structures," in *Electronics Packaging Technology, 2003 5th Conference (EPTC 2003)* , vol., no., pp.533-537, 10-12 Dec. 2003.

[27] Bockelman, D.E.; Eisenstadt, W.R., "Combined differential and common-mode scattering parameters: theory and simulation," in *Microwave Theory and Techniques, IEEE Transactions on*, vol.43, no.7, pp.1530-1539, Jul 1995.

[28] Bockelman, D.E.; Eisenstadt, W.R., "Pure-mode network analyzer for on-wafer measurements of mixed-mode S-parameters of differential circuits," in *Microwave Theory and Techniques, IEEE Transactions on*, vol.45, no.7, pp.1071-1077, Jul 1997.

[29] www.ansys.com.

[30] http://transition.fcc.gov/oet/rfsafety/dielectric.html.

[31] http://www.virtualphantoms.org/index.html.

[32] Kaldjob, E.B.; Geck, B.; Eul, H., "Impedance Measurement of Properly Excited Small Balanced Antennas," in *Antennas and Wireless Propagation Letters, IEEE* , vol.8, no., pp.193-195, 2009.

[33] Konya, S.; Sasamori, T.; Tobana, T.; Isota, Y., "Wideband impedance measurement of balanced antenna using the S-parameter method," in *Microwave Conference Proceedings (APMC), 2011 Asia-Pacific* , vol., no., pp.717-720, 5-8 Dec. 2011.

[34] Sasamori, T.; Konya, S.; Tobana, T.; Isota, Y., "Wideband measurement for input impedance of balanced antenna using the S-parameter method," in*Antenna Technology and Applied Electromagnetics (ANTEM), 2012 15th International Symposium on*, vol., no., pp.1-4, 25-28 June 2012.

[35] Zhang, Y.P.; Tu Zhihong, "Measurement of input impedance of differential microstrip antenna by balun method," in *Radio-Frequency Integration Technology (RFIT), 2012 IEEE International Symposium on* , vol., no., pp.137-139, 21-23 Nov. 2012.

[36] www.st.com.